An efficient solution of time domain boundary integral equations for acoustic scattering and its acceleration by Graphics Processing Units

Fang Q. Hu*
Old Dominion University, Norfolk, Virginia, 23529

The present paper is aimed at developing a fast numerical solution of the time domain boundary integral equation (TDBIE) reformulated from the convective wave equation for large scale wave scattering and propagation problems. Historically, numerical solutions of boundary integral equation in the time domain have encountered two major difficulties. The first is the intrinsic numerical instability in the early time domain boundary integral equation formulations. And the second is the formidably high computational cost associated with the direct solution of the time-domain boundary integral equation. In this paper, both issues are addressed. A stable Burton-Miller type formulation is proposed for the time domain boundary integral equation in the presence of a mean flow. A justification for stability through the energy equation associated with the convective wave equation is given. A comparison of the current formulation with a previous one in literature is also offered. The boundary integral equation is solved by a time domain boundary element method (TDBEM), using high-order basis functions and unstructured surface elements. To significantly reduce the computational cost, a Time Domain Propagation and Distribution (TDPD) algorithm is proposed, making use of the delay- and amplitude-compensated field with a mean flow. Implemented in multi-level interactions, the current algorithm shows a computational cost of $O(N^{1.25})$ per time step where N is the total number of unknowns on surface elements. Furthermore, GPU computing has been utilized to speedup the computation. Numerical aspects of the GPU computing for boundary element solutions are discussed. Comparison with CPU executions is also given. Numerical examples that demonstrate the capabilities of the proposed method are presented.

I. Introduction

Currently, it is still computationally challenging to calculate accurately sound scattering by an acoustically large body at mid to high frequencies. Such a computation is important for studies on noise shielding effects and noise reduction treatments. To resolve acoustic waves at mid to high acoustic frequencies, the total number of nodes on the surface of the body, could be in the orders of $10^7 \sim 10^8$. With such a large number of nodes on the surface alone, volume-based methods, such as finite difference and finite element methods, may not yet be practical for routine applications due to limitations in available computational power and memory storage. Surface-based methods, such as the Boundary Element Method (BEM), may offer a viable approach for accurate solutions. With recent advances in High Performance Computing (HPC), including massively parallel CPUs and GPUs (Graphic Processing Units), and advances in multi-level fast integral equation methods, a time domain fast scattering solution is increasingly becoming a possibility.

For the wave equation in the frequency domain, fast numerical solution of boundary integral equations has been studied extensively in literature. For instance, the Fast Multipole Method (FMM) provides a rapid

^{*}Professor, Department of Mathematics and Statistics, AIAA Associate Fellow

acceleration of the BEM for the Helmholtz equation. 11,22,23 In this approach, the linear system formed in the Boundary Element Method is solved by an iterative solver, in which the matrix vector multiplication, typically of $O(N^2)$ complexity, is accelerated by Fast Multipole Method to a reduced O(N) complexity, where N is the total number of unknowns. Recently developed wideband FMM can effectively deal with high and low frequency waves. 11,24 Other non-multipole based fast methods have also be vigorously developed in the literature. 1,5,6,65

Compared to the frequency domain solutions, time domain Boundary Element Method for the wave equation has received far less attention in the literature. The present paper is aimed at developing a fast numerical solution of the *time domain* boundary integral equation (TDBIE) reformulated for the convective wave equation for large scale wave scattering and propagation problems. A time domain solution has several distinct advantages:

- 1. Broadband sources and time dependent transient signals can be simulated and studied;
- 2. Scattering solutions at all frequencies are obtained within one single computation;
- 3. It can be coupled naturally with nonlinear computations where many frequencies are generated;
- 4. Inversion of a large dense linear system is avoided;
- 5. There are many applications where a time domain solution is preferred, such as in interior acoustics, simulation of time reversal problems, etc.

Although research on time domain boundary element method for wave equation was started in the 60s, 19,49,60 historically, its development has been hindered by two major difficulties. The first is the intrinsic numerical instability in the early time domain boundary integral equation formulations. The instability is attributed to the excitation of the interior resonant modes that are inevitably excited when a transient signal containing a continuous spectrum is introduced in the computation. The second is the formidably high computational cost associated with the direct solution of the time-domain boundary integral equation which scales as $O(N_t N^2)$, where N_t is the total number of time steps. These difficulties presented barriers for applications of the time domain BEM to large scale real-world problems.

In recent years, due to continued research efforts, substantial progresses in time domain BEM have been made. The instability problem has been largely improved. For the wave equation without a convection velocity, an effective way to avoid the instability is to use the Burton-Miller type formulation in the time domain. ^{10,14,36} In [10], the stability of the formulation was shown theoretically. In [36], the formulation was extended to the use of high-order basis functions with an explicit treatment of the hypersingularity in the Burton-Miller type integral equation. Additionally, time discretization based on the so-called convolution quadrature has also been shown to be unconditionally stable when it is coupled with a Galerkin spatial discretization. ^{3,12,28,59} A stabilized time marching scheme significantly broadens the applicability of the time-domain boundary element approach both in the geometrical shape of the body and in the range of frequencies that can be included in the calculation.

Furthermore, in the last decade, methods aimed at reducing the computational complexity of time domain integral equations have also been developed. In particular, two interesting fast methods for time domain integral equations have been proposed in the literature. One is the multi-level Plane Wave Time Domain (PWTD) algorithm, which is akin to the Fast Multipole Method (FMM) in the frequency domain. ^{15,22} The second is the multi-level Cartesian Non-uniform Grid Time Domain algorithm (CNGTDA) based on far-field smoothness of the wave equation kernel. ^{4,40,47} In both approaches, the computational complexity can be reduced formally from $O(N_tN^2)$ to as low as $O(N_tN\log^2 N)$, where N_t is the number of time steps and N is the total number of unknowns. In the present paper, a new, and simplified, algorithm that exploits far field smoothness of the kernel is proposed.

With the advances in stability and fast multi-level numerical methods as well as the emergence of massively parallel computational architectures like GPUs (Graphics Processing Unit), fast and efficient solution of time domain boundary integral equations for large scale real-world applications is increasingly becoming a

possibility. In this paper, a formulation of stable time domain boundary integral equation for the convective wave is proposed and its efficient solution based on a multi-level Cartesian Non-uniform Grid Time Domain method is developed. In addition, application of the recently emerged General Purpose GPU (GPGPU) computing techniques has also been considered for the time domain boundary element method.

The rest of the paper is organized as follows. In section 2, derivation of the time domain boundary integral equation in the presence of a mean flow is given and a stable Burton-Miller type formulation is proposed. A theoretical justification for stability is also presented and a comparison with a previous Kirchhoff formulation is offered. In section 3, the time domain boundary element method is described. A time domain algorithm to significantly reduce the computational complexity is proposed and described in section 4. In section 5, use of GPUs for accelerating the computation is discussed and a comparison with CPU only approach is given. Several numerical examples are presented in section 6. Section 7 contains the conclusions of this study.

II. Derivation of Time Domain Boundary Integral Equation for scattering in the presence of a mean flow and its stability

In this section, the time domain boundary integral equation for scattering with a uniform mean flow is derived. In particular, a new boundary integral equation based on the Burton-Miller type formulation is proposed. Stability of the new formulation is discussed. Comparisons of the current formulation with the previously well-known formulations in aeroacoustics are also given.

A. Time domain Kirchhoff formulation in the presence of a mean flow

Consider the convective wave equation with a constant mean flow U written as

$$\left(\frac{\partial}{\partial t} + \boldsymbol{U} \cdot \nabla\right)^2 p - c^2 \nabla^2 p = q(\boldsymbol{r}, t) \tag{1}$$

with homogeneous initial condition

$$p(\mathbf{r},0) = \frac{\partial p}{\partial t}(\mathbf{r},0) = 0, \quad t = 0$$
(2)

Here q(r,t) represents the source term. The current problem is considered in the context of finding the acoustic solution exterior of certain specified surface, or a collection of surfaces, S, such as the scattered sound field by a aircraft as shown in Figure 1. The formulation of the problem is to be completed with specified boundary conditions on physical surfaces or control surfaces.

To reformulate the wave propagation problem, the PDE (1), the initial condition (2) as well as the boundary conditions, into an integral equation, we introduce the Green's function $\tilde{G}(\mathbf{r},t;\mathbf{r}',t')$ to the adjoint equation defined as follows:

$$\left(\frac{\partial}{\partial t} + \boldsymbol{U} \cdot \nabla\right)^{2} \tilde{G} - c^{2} \nabla^{2} \tilde{G} = \delta(\boldsymbol{r} - \boldsymbol{r}') \delta(t - t')$$
(3)

and initial condition

$$\tilde{G}(\mathbf{r}, t; \mathbf{r}', t') = \frac{\partial \tilde{G}}{\partial t}(\mathbf{r}, t; \mathbf{r}', t') = 0, \quad t > t'$$
(4)

Note that the time domain adjoint Green's function $\tilde{G}(\mathbf{r},t;\mathbf{r}',t')$ is non-zero only for $t \in (-\infty,t']$.

By the operation of $\tilde{G}\times(1)$ - $p\times(3)$ and by using the following properties of the differential operators for any two functions u and p,

$$u\nabla^2 p - p\nabla^2 u = \nabla \cdot (u\nabla p - p\nabla u)$$

and

$$u\left(\frac{\partial}{\partial t} + \boldsymbol{U} \cdot \nabla\right)^{2} p - p\left(\frac{\partial}{\partial t} + \boldsymbol{U} \cdot \nabla\right)^{2} u = \frac{\partial}{\partial t} \left[u\left(\frac{\partial}{\partial t} + \boldsymbol{U} \cdot \nabla\right) p - p\left(\frac{\partial}{\partial t} + \boldsymbol{U} \cdot \nabla\right) u \right] + \nabla \cdot \left\{ \left[u\left(\frac{\partial}{\partial t} + \boldsymbol{U} \cdot \nabla\right) p - p\left(\frac{\partial}{\partial t} + \boldsymbol{U} \cdot \nabla\right) u \right] \boldsymbol{U} \right\}$$

we get

$$\int_{0^{-}}^{t'^{+}} \int_{V} \left\{ \frac{\partial}{\partial t} \left[\tilde{G} \left(\frac{\partial}{\partial t} + \boldsymbol{U} \cdot \nabla \right) p - p \left(\frac{\partial}{\partial t} + \boldsymbol{U} \cdot \nabla \right) \tilde{G} \right] + \nabla \cdot \left[\tilde{G} \left(\frac{\partial}{\partial t} + \boldsymbol{U} \cdot \nabla \right) p - p \left(\frac{\partial}{\partial t} + \boldsymbol{U} \cdot \nabla \right) \tilde{G} \right] \boldsymbol{U} \right\} d\boldsymbol{r} dt = \int_{0^{-}}^{t'^{+}} \int_{V} \left[\tilde{G} q(\boldsymbol{r}, t) - p(\boldsymbol{r}, t) \delta(\boldsymbol{r} - \boldsymbol{r}') \delta(t - t') \right] d\boldsymbol{r} dt$$

Since the first term in the above will be zero by initial conditions, we get an expression for pressure p at an arbitrary point r' and time t' as

$$\begin{split} p(\boldsymbol{r}',t') &= \int_{0^{-}}^{t'^{+}} \int_{V} \tilde{G}q(\boldsymbol{r},t) d\boldsymbol{r} dt + c^{2} \int_{0^{-}}^{t'^{+}} \int_{V} \nabla \cdot (\tilde{G}\nabla p - p\nabla \tilde{G}) d\boldsymbol{r} dt \\ &- \int_{0^{-}}^{t'^{+}} \int_{V} \nabla \cdot \left\{ \left[\tilde{G} \left(\frac{\partial}{\partial t} + \boldsymbol{U} \cdot \nabla \right) p - p \left(\frac{\partial}{\partial t} + \boldsymbol{U} \cdot \nabla \right) \tilde{G} \right] \bar{\boldsymbol{U}} \right\} d\boldsymbol{r} dt \end{split}$$

The integrals in the second and third terms above can be readily converted to surface integrals by using the Divergence Theorem, which yields

$$p(\mathbf{r}',t') = \int_{0^{-}}^{t'^{+}} \int_{V} \tilde{G}q(\mathbf{r},t)d\mathbf{r}dt + c^{2} \int_{0^{-}}^{t'^{+}} \int_{S} (\tilde{G}\frac{\partial p}{\partial n} - p\frac{\partial \tilde{G}}{\partial n})d\mathbf{r}_{s}dt$$
$$-\int_{0^{-}}^{t'^{+}} \int_{S} \left[\tilde{G}\left(\frac{\partial p}{\partial t} + \mathbf{U} \cdot \nabla p\right) - p\left(\frac{\partial \tilde{G}}{\partial t} + \mathbf{U} \cdot \nabla \tilde{G}\right) \right] U_{n}d\mathbf{r}_{s}dt \tag{5}$$

where r_s denotes points on surface S, and

$$U_n = \boldsymbol{n} \cdot \boldsymbol{U}$$

is the normal component of the mean velocity on surface point r_s . In this work, the unit normal vector n is assumed to be *outward from the solution domain*. For the exterior scattering problem, the normal vector is then the one that is inward to the body.

For convenience of discussion, we introduce a modified normal derivative as

$$\frac{\partial}{\partial \bar{n}} = \frac{\partial}{\partial n} - M_n(\mathbf{M} \cdot \nabla) = (\mathbf{n} - M_n \mathbf{M}) \cdot \nabla$$
, and $\bar{\mathbf{n}} = \mathbf{n} - M_n \mathbf{M}$

Then, equation (5) can be written as

$$p(\mathbf{r}',t') = \int_{0}^{t'^{+}} \int_{V} \tilde{G}q(\mathbf{r},t)d\mathbf{r}dt + c^{2} \int_{0}^{t'^{+}} \int_{S} (\tilde{G}\frac{\partial p}{\partial \bar{n}} - p\frac{\partial \tilde{G}}{\partial \bar{n}})d\mathbf{r}_{s}dt - \int_{0}^{t'^{+}} \int_{S} \left[\tilde{G}\frac{\partial p}{\partial t} - p\frac{\partial \tilde{G}}{\partial t} \right] U_{n}d\mathbf{r}_{s}dt \quad (6)$$

Furthermore, if we define

$$\frac{\partial}{\partial \tilde{n}} = \frac{\partial}{\partial \bar{n}} - M_n \frac{1}{c} \frac{\partial}{\partial t}$$

we get

$$p(\mathbf{r}',t') = \int_{0^{-}}^{t'^{+}} \int_{V} \tilde{G}q(\mathbf{r},t)d\mathbf{r}dt + c^{2} \int_{0^{-}}^{t'^{+}} \int_{S} (\tilde{G}\frac{\partial p}{\partial \tilde{n}} - p\frac{\partial \tilde{G}}{\partial \tilde{n}})d\mathbf{r}_{s}dt$$
 (7)

Equation (5), (6) or (7) is the Kirchhoff representation of the acoustic field in the presence of a mean flow. For simplicity, in what follows, we consider the case where the mean flow is along the x axis,

$$U = (U, 0, 0)$$

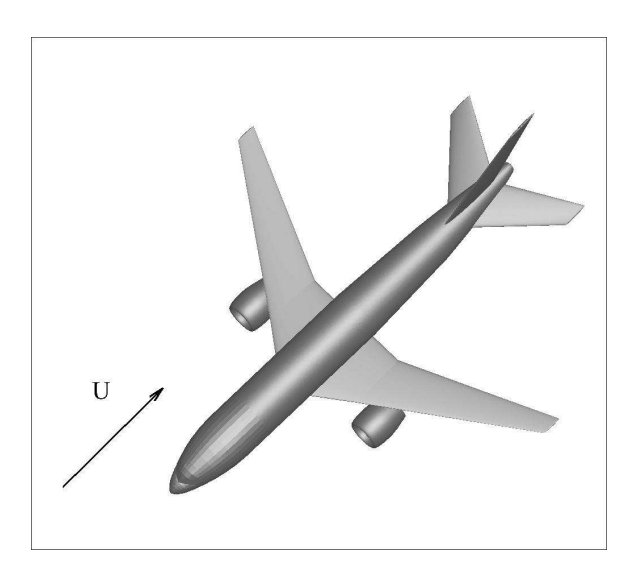


Figure 1. A schematic showing the scattering body and mean flow.

Under this condition, the free space Green's function of the adjoint equation (3) is well-known and can be written as 53,54

$$\tilde{G}(\mathbf{r}, t; \mathbf{r}', t') = \frac{G_0}{4\pi c^2} \delta\left(t' - t + \beta \cdot (\mathbf{r}' - \mathbf{r}) - \frac{\bar{R}}{c\alpha^2}\right)$$
(8)

where

$$G_0 = \frac{1}{\bar{R}(\mathbf{r}, \mathbf{r}')}, \text{ and } \bar{R}(\mathbf{r}, \mathbf{r}') = \sqrt{(x - x')^2 + \alpha^2 (y - y')^2 + \alpha^2 (z - z')^2}$$
 (9)

in which

$$\alpha = \sqrt{1 - (U/c)^2} = \sqrt{1 - M^2}, \ \beta = \frac{U}{c^2 - U^2} = \frac{U}{c^2 \alpha^2} = \frac{M}{c\alpha^2}$$
 (10)

The arguments for $\bar{R}(\mathbf{r}, \mathbf{r}')$ will be omitted when there is no misunderstanding for doing so. Utilizing (8), the integral relation (5) can be expressed in integrations of retarded values on the surfaces only. In particular, note that

$$\nabla \tilde{G} = \frac{1}{4\pi c^2} (\nabla G_0) \delta \left(t' - t + \boldsymbol{\beta} \cdot (\boldsymbol{r}' - \boldsymbol{r}) - \frac{\bar{R}}{c\alpha^2} \right) + \frac{1}{4\pi c^2} G_0 \delta' \left(t' - t + \boldsymbol{\beta} \cdot (\boldsymbol{r}' - \boldsymbol{r}) - \frac{\bar{R}}{c\alpha^2} \right) \left[-\boldsymbol{\beta} - \frac{1}{c\alpha^2} (\nabla \bar{R}) \right]$$

$$\frac{\partial \tilde{G}}{\partial n} = \frac{1}{4\pi c^2} \frac{\partial G_0}{\partial n} \delta \left(t' - t + \boldsymbol{\beta} \cdot (\boldsymbol{r}' - \boldsymbol{r}) - \frac{\bar{R}}{c\alpha^2} \right) + \frac{1}{4\pi c} G_0 \delta' \left(t' - t + \boldsymbol{\beta} \cdot (\boldsymbol{r}' - \boldsymbol{r}) - \frac{\bar{R}}{c\alpha^2} \right) \left[-\boldsymbol{\beta} \cdot \boldsymbol{n} - \frac{1}{c\alpha^2} \frac{\partial \bar{R}}{\partial n} \right]$$

Then equation (5) becomes

$$p(\mathbf{r}',t') = \frac{1}{4\pi c^2} \int_{V} \frac{1}{\bar{R}} q(\mathbf{r},t'_R) d\mathbf{r} + \frac{1}{4\pi c^2} \int_{S} \left[c^2 G_0 \frac{\partial p}{\partial n} (\mathbf{r}_s,t'_R) - c^2 \frac{\partial G_0}{\partial n} p(\mathbf{r}_s,t'_R) - c^2 G_0 \left(-\boldsymbol{\beta} \cdot \mathbf{n} - \frac{1}{c\alpha^2} \frac{\partial \bar{R}}{\partial n} \right) \frac{\partial p}{\partial t} (\mathbf{r}_s,t'_R) \right] d\mathbf{r}_s$$

$$-U_n G_0 \left[\mathbf{U} \cdot \nabla p(\mathbf{r}_s,t'_R) \right] + U_n (\mathbf{U} \cdot \nabla G_0) p(\mathbf{r}_s,t'_R) + U_n G_0 \left[-2 - \boldsymbol{\beta} \cdot \mathbf{U} - \frac{1}{c\alpha^2} (\mathbf{U} \cdot \nabla \bar{R}) \right] \frac{\partial p}{\partial t} (\mathbf{r}_s,t'_R) \right] d\mathbf{r}_s$$

where the retarded time for t' has been denoted by

$$t_R' = t' + \beta \cdot (\mathbf{r}' - \mathbf{r}) - \bar{R}/c\alpha^2 \tag{11}$$

Note also that

$$c^{2}\left(-\boldsymbol{\beta}\cdot\boldsymbol{n}\right)+2U_{n}+\left(\boldsymbol{\beta}\cdot\boldsymbol{U}\right)U_{n}=-\frac{c^{2}U_{n}}{c^{2}\alpha^{2}}+2U_{n}+\frac{U^{2}}{c^{2}\alpha^{2}}U_{n}=U_{n}$$
(12)

and further, if we decompose mean flow U as

$$\boldsymbol{U} = U_n \boldsymbol{n} + \boldsymbol{U}_T \tag{13}$$

where U_T is the tangential component of U, we have

$$p(\mathbf{r}',t') = \frac{1}{4\pi c^2} \int_{V} \frac{1}{\bar{R}} q(\mathbf{r},t'_R) d\mathbf{r} + \frac{1}{4\pi c^2} \int_{S} \left[\left(c^2 - U_n^2 \right) G_0 \frac{\partial p}{\partial n} (\mathbf{r}_s,t'_R) - \left(c^2 \frac{\partial G_0}{\partial n} - U_n(\mathbf{U} \cdot \nabla G_0) \right) p(\mathbf{r}_s,t'_R) \right] - U_n G_0 \left(\mathbf{U}_T \cdot \nabla p(\mathbf{r}_s,t'_R) \right) + G_0 \left[\frac{1}{c\alpha^2} \left(c^2 \frac{\partial \bar{R}}{\partial n} - U_n(\mathbf{U} \cdot \nabla \bar{R}) \right) - U_n \right] \frac{\partial p}{\partial t} (\mathbf{r}_s,t'_R) \right] d\mathbf{r}_s$$

To further simplify the expressions, we note these modified normal derivatives:

$$\frac{\partial \bar{R}}{\partial \bar{n}} \equiv \frac{\partial \bar{R}}{\partial n} - M_n(\mathbf{M} \cdot \nabla \bar{R}) = \alpha^2 \frac{n_1(x - x') + n_2(y - y') + n_3(z - z')}{\bar{R}} = \alpha^2 \frac{\mathbf{n} \cdot (\mathbf{r} - \mathbf{r}')}{\bar{R}}$$

$$\frac{\partial G_0}{\partial \bar{n}} \equiv \frac{\partial G_0}{\partial n} - M_n(\mathbf{M} \cdot \nabla G_0) = -\alpha^2 \frac{n_1(x - x') + n_2(y - y') + n_3(z - z')}{\bar{R}^3} = -\alpha^2 \frac{\mathbf{n} \cdot (\mathbf{r} - \mathbf{r}')}{\bar{R}^3}$$

Finally, the Kirchhoff integral relation (5) can be written as

$$4\pi p(\mathbf{r}', t') = \frac{1}{c^2} \int_{V} \frac{1}{\bar{R}} q(\mathbf{r}, t'_R) d\mathbf{r} + \int_{S} \left[\left(1 - M_n^2 \right) G_0 \frac{\partial p}{\partial n} (\mathbf{r}_s, t'_R) - \frac{\partial G_0}{\partial \bar{n}} p(\mathbf{r}_s, t'_R) \right] - M_n G_0 \left(\mathbf{M}_T \cdot \nabla p(\mathbf{r}_s, t'_R) \right) + \frac{1}{c\alpha^2} G_0 \left(\frac{\partial \bar{R}}{\partial \bar{n}} - \alpha^2 M_n \right) \frac{\partial p}{\partial t} (\mathbf{r}_s, t'_R) d\mathbf{r}_s$$

$$(14)$$

By equation (14), solution at any point \mathbf{r}' and time t' is related to the direct contribution from the source function q and a surface integral involving the retarded pressure and its normal derivative. In other words, if both $p(\mathbf{r}_s,t)$ and $\frac{\partial p}{\partial n}(\mathbf{r}_s,t)$ are known, then $p(\mathbf{r}',t')$ can be computed by using (14). However, p and $\frac{\partial p}{\partial n}$ are not independent. They have to satisfy the boundary integral equation formed when \mathbf{r}' is taken to be a boundary point \mathbf{r}'_s as we will see next.

B. Derivation of boundary integral equation

To derive the boundary integral equation, consider the limit $\mathbf{r'} \to \mathbf{r'_s}$ for equation (14), where $\mathbf{r'_s}$ is a point on the boundary. Special attention is needed for the term involving $\frac{\partial G_0}{\partial \bar{n}}$, where the integral becomes singular and the limit can not be directly interchanged with the integration. This particular limit has been studied in the literature. To properly find the limit, consider modifying surface S by a spherical surface centered at $\mathbf{r'_s}$ as shown in Figure 2. Specifically, if we denote the small spherical surface as S_{ϵ} , we proceed as

$$\lim_{\mathbf{r}' \to \mathbf{r}'_{s}} \int_{S} \frac{\partial G_{0}}{\partial \bar{n}}(\mathbf{r}_{s}, \mathbf{r}') p(\mathbf{r}_{s}, t'_{R}) d\mathbf{r}_{s} = \lim_{\mathbf{r}' \to \mathbf{r}'_{s}} \int_{S - S_{\epsilon}} \frac{\partial G_{0}}{\partial \bar{n}}(\mathbf{r}_{s}, \mathbf{r}') p(\mathbf{r}_{s}, t'_{R}) d\mathbf{r}_{s}$$

$$+ \lim_{\mathbf{r}' \to \mathbf{r}'_{s}} \int_{S_{\epsilon}} \frac{\partial G_{0}}{\partial \bar{n}}(\mathbf{r}_{s}, \mathbf{r}') \left[p(\mathbf{r}_{s}, t'_{R}) - p(\mathbf{r}'_{s}, t') \right] d\mathbf{r}_{s} + p(\mathbf{r}'_{s}, t') \lim_{\mathbf{r}' \to \mathbf{r}'_{s}} \int_{S_{\epsilon}} \frac{\partial G_{0}}{\partial \bar{n}}(\mathbf{r}_{s}, \mathbf{r}') d\mathbf{r}_{s}$$

$$(15)$$

Note that, for the surface integral on S_{ϵ} , we have

$$\frac{\partial G_0}{\partial \bar{p}} = -\alpha^2 \frac{n_1(x_s - x_s') + n_2(y_s - y_s') + n_3(z_s - z_s')}{\bar{p}^3} = -\alpha^2 \frac{\epsilon}{\bar{p}^3}$$

and

$$\lim_{\mathbf{r}' \to \mathbf{r}'_s} \int_{S_{\epsilon}} \frac{\partial G_0}{\partial \bar{n}} d\mathbf{r}_s = -\alpha^2 \int_{S_{\epsilon}} \frac{\epsilon}{\bar{R}^3} d\mathbf{r}_s = -\alpha^2 \int_{S_{\epsilon}} \frac{\epsilon}{((x_s - x'_s)^2 + \alpha^2 (y_s - y'_s)^2 + \alpha^2 (z_s - z'_s)^2)^{3/2}} d\mathbf{r}_s$$

When r'_s is a point on a smooth surface, S_{ϵ} is a hemisphere. By the symmetry of \bar{R} with respect to hemispheres S_{ϵ} and S'_{ϵ} , the complementary hemisphere of S_{ϵ} , and by using a spherical coordinate centered at r'_s , namely $x_s - x'_s = \epsilon \cos \phi$, $y_s - y'_s = \epsilon \sin \phi \cos \theta$, $z_s - z'_s = \epsilon \sin \phi \sin \theta$, we have

$$\lim_{\mathbf{r}' \to \mathbf{r}'_s} \int_{S_{\epsilon}} \frac{\partial G_0}{\partial \bar{n}} d\mathbf{r}_s = -\alpha^2 \int_{S_{\epsilon}} \frac{\epsilon}{\bar{R}^3} d\mathbf{r}_s = -\frac{\alpha^2}{2} \int_{S_{\epsilon} + S'_{\epsilon}} \frac{\epsilon}{\bar{R}^3} d\mathbf{r}_s = -\frac{\alpha^2}{2} \int_0^{2\pi} \int_0^{\pi} \frac{\epsilon^3 \sin \phi}{\left(\epsilon^2 \cos^2 \phi + \epsilon^2 \alpha^2 \sin^2 \phi\right)^{3/2}} d\phi d\theta$$
$$= -\pi \alpha^2 \int_{-1}^{1} \frac{1}{\left(\alpha^2 + (1 - \alpha^2)t^2\right)^{3/2}} dt = -2\pi$$

The last integral above can be found by direct integration.

Thus, as $\epsilon \to 0$, following (15), we have

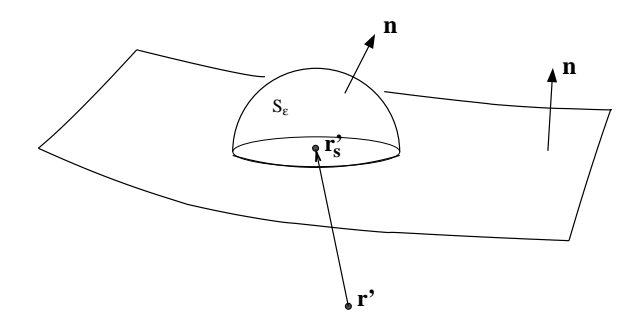


Figure 2. A schematic diagram for a hemisphere that caps a surface point r'_s . Note that the normal vector is in the direction outward from the region of solution and into the body.

$$\lim_{\mathbf{r}' \to \mathbf{r}'_s} \int_{S} \frac{\partial G_0}{\partial \bar{n}}(\mathbf{r}_s, \mathbf{r}') p(\mathbf{r}_s, t'_R) d\mathbf{r}_s = \int_{S} \frac{\partial G_0}{\partial \bar{n}}(\mathbf{r}_s, \mathbf{r}'_s) p(\mathbf{r}_s, t'_R) d\mathbf{r}_s - 2\pi p(\mathbf{r}'_s, t')$$
(16)

Applying this limit to (14), we get the Boundary Integral Equation as follows:

$$2\pi p(\mathbf{r}'_{s}, t') = \frac{1}{c^{2}} \int_{V} \frac{1}{\bar{R}} q(\mathbf{r}'_{s}, t'_{R}) d\mathbf{r} + \int_{S} \left[\left(1 - M_{n}^{2} \right) G_{0} \frac{\partial p}{\partial n} (\mathbf{r}_{s}, t'_{R}) - \frac{\partial G_{0}}{\partial \bar{n}} p(\mathbf{r}_{s}, t'_{R}) - \frac{\partial G_{0}}{\partial \bar{n}} p(\mathbf{r}_{s}, t'_{R}) \right] d\mathbf{r}_{s}$$

$$-M_{n} G_{0} \left(\mathbf{M}_{T} \cdot \nabla p(\mathbf{r}_{s}, t'_{R}) \right) + \frac{1}{c\alpha^{2}} G_{0} \left(\frac{\partial \bar{R}}{\partial \bar{n}} - \alpha^{2} M_{n} \right) \frac{\partial p}{\partial t} (\mathbf{r}_{s}, t'_{R}) d\mathbf{r}_{s}$$

$$(17)$$

On a solid surface, we have $\frac{\partial p}{\partial n} = 0$. Equation (17) can be used to solve for $p(\mathbf{r}'_s, t')$. Then, by using (14), solutions at any field point (\mathbf{r}', t') can be obtained.

C. Derivation of Burton-Miller formulation in time domain with a mean flow

It is well known that integral equation solution by the boundary element method for the exterior scattering problem can lead to numerical instability. The instability is generally attributed to the existence of resonance frequencies for the interior domain. ^{14,53,63,64} In the frequency domain solutions, common remedies include the Burton-Miller formulation, where the boundary integral equation is reformulated using a combination of the single and double layer potentials, and the CHIEF method, where additional collocation points from the interior domain are added to the boundary integral equation. In time domain solutions, the instability is more prevalent as a continuous spectrum of frequencies within the numerical resolution are present in the calculation. This instability has been a major difficulty for the use of time domain integral equations. Recently, progresses have been made in eliminating the numerical instability. In [14], a Burton-Miller type formulation has been used for the March-On-in-Time solution of the time domain integral equation for the wave equation, where the new integral equation is formed by a linear combination of the time and normal derivatives of the original boundary integral equation. In [10], a theoretical justification has been provided for the extension of the Burton-Miller formulation to the time domain for the wave equation without flow.

In this paper, it is proposed that the Burton-Miller type formulation for the time domain boundary integral equation in the presence of a mean flow be formed by a linear combination of the time and *modified normal derivatives* of the boundary integral equation. Use of the modified normal derivative was also suggested in an earlier work in a frequency domain formulation.⁶⁴ To the author's knowledge, such a formulation for the time domain is new and has not been studied previously in the literature. A theoretical justification will be given in the next section.

To facilitate the derivation of the reformulation, we express the time domain integral relations (14) and (17) as

$$4\pi C_s p(\mathbf{r}', t') = \frac{1}{c^2} \int_V \frac{1}{\bar{R}} q(\mathbf{r}', t_R') d\mathbf{r} + \int_S \left[\left(1 - M_n^2 \right) G_0 \frac{\partial p}{\partial n} (\mathbf{r}_s, t_R') - \frac{\partial G_0}{\partial \bar{n}} \left(p(\mathbf{r}_s, t_R') + \frac{\bar{R}}{c\alpha^2} \frac{\partial p}{\partial t} (\mathbf{r}_s, t_R') \right) - M_n G_0 \left(\mathbf{M}_T \cdot \nabla p(\mathbf{r}_s, t_R') + \frac{1}{c} \frac{\partial p}{\partial t} (\mathbf{r}_s, t_R') \right) \right] d\mathbf{r}_s$$

$$(18)$$

where

$$C_s = \begin{cases} 1 & \mathbf{r}' \text{ exterior of } S \\ \frac{1}{2} & \mathbf{r}' \text{ on } S \text{ (smooth points)} \end{cases}$$

With an application of the boundary condition $\frac{\partial p}{\partial n} = 0$ for the problem of scattering by bodies with solid surfaces, equation (18) becomes

$$4\pi C_s p(\mathbf{r}', t') = \frac{1}{c^2} \int_V \frac{1}{\bar{R}} q(\mathbf{r}', t'_R) d\mathbf{r} - \int_S \left[\frac{\partial G_0}{\partial \bar{n}} \left(p(\mathbf{r}_s, t'_R) + \frac{\bar{R}}{c\alpha^2} \frac{\partial p}{\partial t} (\mathbf{r}_s, t'_R) \right) + M_n G_0 \left(\mathbf{M}_T \cdot \nabla p(\mathbf{r}_s, t'_R) + \frac{1}{c} \frac{\partial p}{\partial t} (\mathbf{r}_s, t'_R) \right) \right] d\mathbf{r}_s$$
(19)

Taking a derivative of the above in the form of

$$a\frac{\partial}{\partial t'} + bc\frac{\partial}{\partial \bar{n}'} \tag{20}$$

where a and b are constants and c is the speed of sound, the Burton-Miller formulation leads to the following

$$4\pi a C_{s} \frac{\partial p(\mathbf{r}'_{s}, t')}{\partial t} + 4\pi b c \frac{\partial C_{s}}{\partial \bar{n}'} p(\mathbf{r}'_{s}, t') + 4\pi b c C_{s} \frac{\partial p(\mathbf{r}'_{s}, t')}{\partial \bar{n}'}$$

$$= a \frac{1}{c^{2}} \int_{V} \frac{1}{\bar{R}} \frac{\partial q}{\partial t} (\mathbf{r}'_{s}, t'_{R}) d\mathbf{r} + \frac{b}{c} \frac{\partial}{\partial \bar{n}'} \int_{V} \frac{1}{\bar{R}} q(\mathbf{r}'_{s}, t'_{R}) d\mathbf{r}$$

$$-a \int_{S} \left[\frac{\partial G_{0}}{\partial \bar{n}} \left(\frac{\partial p}{\partial t} (\mathbf{r}_{s}, t'_{R}) + \frac{\bar{R}}{c\alpha^{2}} \frac{\partial^{2}p}{\partial t^{2}} (\mathbf{r}_{s}, t'_{R}) \right) + M_{n} G_{0} \left(\mathbf{M}_{T} \cdot \nabla \frac{\partial p}{\partial t} (\mathbf{r}_{s}, t'_{R}) + \frac{1}{c} \frac{\partial^{2}p}{\partial t^{2}} (\mathbf{r}_{s}, t'_{R}) \right) \right] d\mathbf{r}_{s}$$

$$-bc \int_{S} \left[\frac{\partial^{2}G_{0}}{\partial \bar{n}' \partial \bar{n}} \left(p(\mathbf{r}_{s}, t'_{R}) + \frac{\bar{R}}{c\alpha^{2}} \frac{\partial p}{\partial t} (\mathbf{r}_{s}, t'_{R}) \right) + M_{n} \frac{\partial G_{0}}{\partial \bar{n}'} \left(\mathbf{M}_{T} \cdot \nabla p(\mathbf{r}_{s}, t'_{R}) + \frac{1}{c} \frac{\partial p}{\partial t} (\mathbf{r}_{s}, t'_{R}) \right) \right] d\mathbf{r}_{s}$$

$$- \frac{b}{\alpha^{2}} \int_{S} \frac{\partial G_{0}}{\partial \bar{n}} \left[\left(\mathbf{M} \cdot \bar{\mathbf{n}}' \right) \frac{\partial p}{\partial t} (\mathbf{r}_{s}, t'_{R}) + \frac{\bar{R}}{c\alpha^{2}} \left(\mathbf{M} \cdot \bar{\mathbf{n}}' - \frac{\partial \bar{R}}{\partial \bar{n}'} \right) \frac{\partial^{2}p}{\partial t^{2}} (\mathbf{r}_{s}, t'_{R}) \right] d\mathbf{r}_{s}$$

$$- \frac{b}{\alpha^{2}} \int_{S} M_{n} G_{0} \left(\mathbf{M} \cdot \bar{\mathbf{n}}' - \frac{\partial \bar{R}}{\partial \bar{n}'} \right) \left(\mathbf{M}_{T} \cdot \nabla \frac{\partial p}{\partial t} (\mathbf{r}_{s}, t'_{R}) + \frac{1}{c} \frac{\partial^{2}p}{\partial t^{2}} (\mathbf{r}_{s}, t'_{R}) \right) d\mathbf{r}_{s}$$

$$- \frac{b}{\alpha^{2}} \int_{S} M_{n} G_{0} \left(\mathbf{M} \cdot \bar{\mathbf{n}}' - \frac{\partial \bar{R}}{\partial \bar{n}'} \right) \left(\mathbf{M}_{T} \cdot \nabla \frac{\partial p}{\partial t} (\mathbf{r}_{s}, t'_{R}) + \frac{1}{c} \frac{\partial^{2}p}{\partial t^{2}} (\mathbf{r}_{s}, t'_{R}) \right) d\mathbf{r}_{s}$$

$$(21)$$

The proper values for the coefficients a and b will be given in the next section following a discussion on the stability. The term with a double normal derivative of the G_0 is hyper-singular. In particular, we have

$$\frac{\partial^2 G_0}{\partial \bar{n}' \partial \bar{n}} = \frac{\partial}{\partial \bar{n}'} \left[-\alpha^2 \frac{n_1(x - x') + n_2(y - y') + n_3(z - z')}{\bar{R}^3} \right]$$

$$= \alpha^2 \frac{n_1 n_1' + n_2 n_2' + n_3 n_3'}{\bar{R}^3} - \frac{M_{n'}(\alpha^2 n_1 M)}{\bar{R}^3} + 3\alpha^2 \frac{\boldsymbol{n} \cdot (\boldsymbol{r} - \boldsymbol{r}')}{\bar{R}^4} \frac{\partial \bar{R}}{\partial \bar{n}'}$$

$$= \alpha^2 \frac{\alpha^2 n_1 n_1' + n_2 n_2' + n_3 n_3'}{\bar{R}^3} + 3\alpha^4 \frac{[\boldsymbol{n} \cdot (\boldsymbol{r} - \boldsymbol{r}')] [\boldsymbol{n}' \cdot (\boldsymbol{r}' - \boldsymbol{r})]}{\bar{R}^5}$$

To deal with the hyper-singular term $\frac{\partial^2 G_0}{\partial \bar{n}' \partial \bar{n}}$, we note the relation

$$4\pi(1 - C_s) = \int_S \frac{\partial G_0}{\partial \bar{n}} d\mathbf{r}_s \tag{22}$$

This equation can be easily justified from the fact that p = 1 is a solution to the interior domain problem with a homogeneous normal derivative boundary condition.

By (22), we have

$$4\pi \frac{\partial C_s}{\partial \bar{n}'} = -\frac{\partial}{\partial \bar{n}'} \int_S \frac{\partial G_0}{\partial \bar{n}} d\mathbf{r}_s = -\int_S \frac{\partial G_0^2}{\partial \bar{n}' \partial \bar{n}} d\mathbf{r}_s \tag{23}$$

Equation (23) can be used utilized to reduce the hyper-singularity of the term with the double normal derivative of G_0 , so that it can be evaluated using the Cauchy principal value (see [10] and the Appendix). By substituting the above into (21) and re-arranging the terms, we get the following Burton-Miller type Boundary Integral Equation:

$$4\pi a C_{s} \frac{\partial p(\mathbf{r}'_{s}, t')}{\partial t} + 4\pi b c C_{s} \frac{\partial p(\mathbf{r}'_{s}, t')}{\partial \bar{n}'} = a \frac{1}{c^{2}} \int_{V} \frac{1}{\bar{R}} \frac{\partial q}{\partial t} (\mathbf{r}'_{s}, t'_{R}) d\mathbf{r} + \frac{b}{c} \frac{\partial}{\partial \bar{n}'} \int_{V} \frac{1}{\bar{R}} \frac{\partial q}{\partial t} (\mathbf{r}'_{s}, t'_{R}) d\mathbf{r}$$

$$-a \int_{S} \left[\frac{\partial G_{0}}{\partial \bar{n}} \left(\frac{\partial p}{\partial t} (\mathbf{r}_{s}, t'_{R}) + \frac{\bar{R}}{c\alpha^{2}} \frac{\partial^{2}p}{\partial t^{2}} (\mathbf{r}_{s}, t'_{R}) \right) + M_{n} G_{0} \left(\mathbf{M}_{T} \cdot \nabla \frac{\partial p}{\partial t} (\mathbf{r}_{s}, t'_{R}) + \frac{1}{c} \frac{\partial^{2}p}{\partial t^{2}} (\mathbf{r}_{s}, t'_{R}) \right) \right] d\mathbf{r}_{s}$$

$$-b c \int_{S} \frac{\partial^{2}G_{0}}{\partial \bar{n}'} \left(p(\mathbf{r}_{s}, t'_{R}) - p(\mathbf{r}'_{s}, t') + \frac{\bar{R}}{c\alpha^{2}} \frac{\partial p}{\partial t} (\mathbf{r}_{s}, t'_{R}) \right) d\mathbf{r}_{s}$$

$$-b c \int_{S} M_{n} \frac{\partial G_{0}}{\partial \bar{n}'} \left(\mathbf{M}_{T} \cdot \nabla p(\mathbf{r}_{s}, t'_{R}) + \frac{1}{c} \frac{\partial p}{\partial t} (\mathbf{r}_{s}, t'_{R}) \right) d\mathbf{r}_{s}$$

$$-\frac{b}{\alpha^{2}} \int_{S} \frac{\partial G_{0}}{\partial \bar{n}} \left[(\mathbf{M} \cdot \bar{\mathbf{n}}') \frac{\partial p}{\partial t} (\mathbf{r}_{s}, t'_{R}) + \frac{\bar{R}}{c\alpha^{2}} \left(\mathbf{M} \cdot \bar{\mathbf{n}}' - \frac{\partial \bar{R}}{\partial \bar{n}'} \right) \frac{\partial^{2}p}{\partial t^{2}} (\mathbf{r}_{s}, t'_{R}) \right] d\mathbf{r}_{s}$$

$$-\frac{b}{\alpha^{2}} \int_{S} M_{n} G_{0} \left(\mathbf{M} \cdot \bar{\mathbf{n}}' - \frac{\partial \bar{R}}{\partial \bar{n}'} \right) \left(\mathbf{M}_{T} \cdot \nabla \frac{\partial p}{\partial t} (\mathbf{r}_{s}, t'_{R}) + \frac{1}{c} \frac{\partial^{2}p}{\partial t^{2}} (\mathbf{r}_{s}, t'_{R}) \right) d\mathbf{r}_{s}$$

$$(24)$$

With the reduction of the singularity, equation (24) is in a form that can be readily used for Boundary Element computations.

To carry out the operation $M_T \cdot \nabla \frac{\partial p}{\partial t}(\mathbf{r}_s, t_R')$, note the decomposition

$$M = M_n n + M_{T1} e_{\varepsilon} + M_{T2} e_n$$

where e_{ξ} and e_{η} are the unit vectors in the local surface coordinates, such that

$$M \cdot n = M_n$$

$$\mathbf{M} \cdot \mathbf{e}_{\varepsilon} = M_{T1} + M_{T2} (\mathbf{e}_{\varepsilon} \cdot \mathbf{e}_{n})$$

$$\mathbf{M} \cdot \mathbf{e}_{\eta} = M_{T1}(\mathbf{e}_{\xi} \cdot \mathbf{e}_{\eta}) + M_{T2}$$

giving

$$M_{T1} = \frac{M \cdot e_{\xi} - (e_{\xi} \cdot e_{\eta})M \cdot e_{\eta}}{1 - (e_{\xi} \cdot e_{\eta})^{2}}$$

$$M_{T2} = \frac{M \cdot e_{\eta} - (e_{\xi} \cdot e_{\eta})M \cdot e_{\xi}}{1 - (e_{\xi} \cdot e_{\eta})^{2}}$$

Then,

$$M_T \cdot \nabla \frac{\partial p}{\partial t}(\boldsymbol{r}_s, t_R') = M_{T1} \frac{\partial}{\partial \varepsilon} \frac{\partial p}{\partial t}(\boldsymbol{r}_s, t_R') + M_{T2} \frac{\partial}{\partial n} \frac{\partial p}{\partial t}(\boldsymbol{r}_s, t_R')$$

where (ξ, η) is the local element coordinate on the surface. The derivatives in the right hand side can be easily computed in local basis functions.

We also note that

$$\frac{\partial p(\boldsymbol{r}_s',t')}{\partial \bar{n}'} = \frac{\partial p(\boldsymbol{r}_s',t')}{\partial n'} - M_{n'}\boldsymbol{M} \cdot \nabla p(\boldsymbol{r}_s',t') = (1 - M_{n'}^2) \frac{\partial p(\boldsymbol{r}_s',t')}{\partial n'} - M_{n'}\boldsymbol{M}_{T'} \cdot \nabla p(\boldsymbol{r}_s',t')$$

D. Stability of the time domain Burton-Miller formulation in the presence of a mean flow

We now consider the stability of the Burton-Miller type formulation given in the previous section. The considerations follows closely those given in [10] for the case without flow. The main point is to demonstrate that with reformulation of the Burton-Miller type, there will be no non-trivial solution for the interior domain, thus eliminating the resonant frequencies.

We first establish an energy equation for the convective wave equation that will be useful in proving the stability of the current formulation. For a solution to the homogeneous convective wave equation,

$$\left(\frac{\partial}{\partial t} + \boldsymbol{U} \cdot \nabla\right)^2 \phi - c^2 \nabla \phi = 0 \tag{25}$$

it can be shown that it has an associated energy equation as

$$\frac{\partial}{\partial t} \left(\frac{1}{2} |\nabla \phi|^2 + \frac{1}{2c^2} \left| \frac{D\phi}{Dt} \right|^2 - \frac{U \cdot \nabla \phi}{c^2} \frac{D\phi}{Dt} \right) + \nabla \cdot \left[-\frac{\partial \phi}{\partial t} \left(\nabla \phi - \frac{1}{c^2} \frac{D\phi}{Dt} U \right) \right] = 0 \tag{26}$$

where

$$\frac{D}{Dt} = \frac{\partial}{\partial t} + \boldsymbol{U} \cdot \nabla$$

Equation (26) can be verified directly for any ϕ that satisfies (25). Equation (26) can also be inferred from the well-known results on acoustic energy equations.^{50,52}

Now suppose that there is a non-trivial solution $p_0(\mathbf{r}',t')$ to the homogeneous Burton-Miller formulation (24):

$$a\frac{\partial}{\partial t} \left\{ 4\pi C_s p_0(\mathbf{r}'_s, t') + \int_S \left[\frac{\partial G_0}{\partial \bar{n}} \left(p(\mathbf{r}_s, t'_R) + \frac{\bar{R}}{c\alpha^2} \frac{\partial p_0}{\partial t} (\mathbf{r}_s, t'_R) \right) + M_n G_0 \frac{1}{c} \frac{d' p_0}{d't} (\mathbf{r}_s, t'_R) \right] d\mathbf{r}_s \right\}$$

$$+bc \frac{\partial}{\partial \bar{n}'} \left\{ 4\pi C_s p_0(\mathbf{r}'_s, t') + \int_S \left[\frac{\partial G_0}{\partial \bar{n}} \left(p_0(\mathbf{r}_s, t'_R) + \frac{\bar{R}}{c\alpha^2} \frac{\partial p_0}{\partial t} (\mathbf{r}_s, t'_R) \right) + M_n G_0 \frac{1}{c} \frac{d' p_0}{d't} (\mathbf{r}_s, t'_R) \right] d\mathbf{r}_s \right\} = 0$$

$$(27)$$

in which

$$\frac{d'}{d't} = \frac{\partial}{\partial t} + \boldsymbol{U}_T \cdot \nabla$$

We will show in what follows that such a solution is not possible.

Suppose we let

$$Q(\mathbf{r}',t') = \int_{S} \left[\frac{\partial G_0}{\partial \bar{n}} \left(p_0(\mathbf{r}_s,t_R') + \frac{\bar{R}}{c\alpha^2} \frac{\partial p_0}{\partial t}(\mathbf{r}_s,t_R') \right) + M_n G_0 \frac{1}{c} \frac{d' p_0}{d't}(\mathbf{r}_s,t_R') \right] d\mathbf{r}_s$$

It is easily seen that $Q(\mathbf{r}',t')$, now a function of \mathbf{r}' and t' through $\bar{R}(\mathbf{r},\mathbf{r}')$ and t'_R , satisfies the homogeneous wave equation, both in the exterior and interior regions of surface S, due to the integral kernel used. However, $Q(\mathbf{r}',t')$ is not continuous across the surface and, considering the limit (16), the jump conditions at the boundary are

$$Q_{+} - Q_{-} = -4\pi p_{0}$$

$$\frac{\partial Q_+}{\partial \bar{n}'} - \frac{\partial Q_-}{\partial \bar{n}'} = 0$$

where subscripts + and - indicates the solutions exterior and interior of S respectively. After applying these jump conditions to (27), and following the work in [10], we have, on the boundary interior of S,

$$a\frac{\partial}{\partial t}\left\{Q_{-}\right\} + bc\frac{\partial}{\partial \bar{n}'}\left\{Q_{-}\right\} = 0 \tag{28}$$

On the other hand, since Q_{-} satisfies the convective wave equation and by the energy equation (26) of the convective wave equation, we have

$$\frac{\partial}{\partial t} \int_{V} \left[\frac{1}{2} |\nabla Q_{-}|^{2} + \frac{1}{2c^{2}} \left| \frac{DQ_{-}}{Dt} \right|^{2} - \frac{\boldsymbol{U} \cdot \nabla Q_{-}}{c^{2}} \frac{DQ_{-}}{Dt} \right] dV = \int_{V} \nabla \cdot \left[\frac{\partial Q_{-}}{\partial t} \left(\nabla Q_{-} - \frac{1}{c^{2}} \left(\frac{\partial Q_{-}}{\partial t} + \boldsymbol{U} \cdot \nabla Q_{-} \right) \boldsymbol{U} \right) \right] dS + \frac{1}{2c^{2}} \left[\frac{\partial Q_{-}}{\partial t} + \frac{1}{2c^{2}} \left(\frac{\partial Q_{-}}{\partial t} + \boldsymbol{U} \cdot \nabla Q_{-} \right) \boldsymbol{U} \right] dS + \frac{1}{2c^{2}} \left[\frac{\partial Q_{-}}{\partial t} + \frac{1}{2c^{2}} \left(\frac{\partial Q_{-}}{\partial t} + \boldsymbol{U} \cdot \nabla Q_{-} \right) \boldsymbol{U} \right] dS + \frac{1}{2c^{2}} \left[\frac{\partial Q_{-}}{\partial t} + \frac{1}{2c^{2}} \left(\frac{\partial Q_{-}}{\partial t} + \boldsymbol{U} \cdot \nabla Q_{-} \right) \boldsymbol{U} \right] dS + \frac{1}{2c^{2}} \left[\frac{\partial Q_{-}}{\partial t} + \frac{1}{2c^{2}} \left(\frac{\partial Q_{-}}{\partial t} + \boldsymbol{U} \cdot \nabla Q_{-} \right) \boldsymbol{U} \right] dS + \frac{1}{2c^{2}} \left[\frac{\partial Q_{-}}{\partial t} + \frac{1}{2c^{2}} \left(\frac{\partial Q_{-}}{\partial t} + \boldsymbol{U} \cdot \nabla Q_{-} \right) \boldsymbol{U} \right] dS + \frac{1}{2c^{2}} \left[\frac{\partial Q_{-}}{\partial t} + \boldsymbol{U} \cdot \nabla Q_{-} \right] \boldsymbol{U} \right] dS + \frac{1}{2c^{2}} \left[\frac{\partial Q_{-}}{\partial t} + \frac{1}{2c^{2}} \left(\frac{\partial Q_{-}}{\partial t} + \boldsymbol{U} \cdot \nabla Q_{-} \right) \boldsymbol{U} \right] dS + \frac{1}{2c^{2}} \left[\frac{\partial Q_{-}}{\partial t} + \frac{1}{2c^{2}} \left(\frac{\partial Q_{-}}{\partial t} + \boldsymbol{U} \cdot \nabla Q_{-} \right) \boldsymbol{U} \right] dS + \frac{1}{2c^{2}} \left[\frac{\partial Q_{-}}{\partial t} + \frac{1}{2c^{2}} \left(\frac{\partial Q_{-}}{\partial t} + \boldsymbol{U} \cdot \nabla Q_{-} \right) \boldsymbol{U} \right] dS + \frac{1}{2c^{2}} \left[\frac{\partial Q_{-}}{\partial t} + \frac{1}{2c^{2}} \left(\frac{\partial Q_{-}}{\partial t} + \boldsymbol{U} \cdot \nabla Q_{-} \right) \boldsymbol{U} \right] dS + \frac{1}{2c^{2}} \left[\frac{\partial Q_{-}}{\partial t} + \frac{1}{2c^{2}} \left(\frac{\partial Q_{-}}{\partial t} + \boldsymbol{U} \cdot \nabla Q_{-} \right) \boldsymbol{U} \right] dS + \frac{1}{2c^{2}} \left[\frac{\partial Q_{-}}{\partial t} + \frac{1}{2c^{2}} \left(\frac{\partial Q_{-}}{\partial t} + \boldsymbol{U} \cdot \nabla Q_{-} \right) \boldsymbol{U} \right] dS + \frac{1}{2c^{2}} \left[\frac{\partial Q_{-}}{\partial t} + \frac{1}{2c^{2}} \left(\frac{\partial Q_{-}}{\partial t} + \boldsymbol{U} \cdot \nabla Q_{-} \right) \boldsymbol{U} \right] dS + \frac{1}{2c^{2}} \left[\frac{\partial Q_{-}}{\partial t} + \frac{1}{2c^{2}} \left(\frac{\partial Q_{-}}{\partial t} + \boldsymbol{U} \cdot \nabla Q_{-} \right) \boldsymbol{U} \right] dS + \frac{1}{2c^{2}} \left[\frac{\partial Q_{-}}{\partial t} + \frac{1}{2c^{2}} \left(\frac{\partial Q_{-}}{\partial t} + \boldsymbol{U} \cdot \nabla Q_{-} \right) \boldsymbol{U} \right] dS + \frac{1}{2c^{2}} \left[\frac{\partial Q_{-}}{\partial t} + \frac{1}{2c^{2}} \left(\frac{\partial Q_{-}}{\partial t} + \boldsymbol{U} \cdot \nabla Q_{-} \right) \boldsymbol{U} \right] dS + \frac{1}{2c^{2}} \left[\frac{\partial Q_{-}}{\partial t} + \frac{1}{2c^{2}} \left(\frac{\partial Q_{-}}{\partial t} + \boldsymbol{U} \cdot \nabla Q_{-} \right) \boldsymbol{U} \right] dS + \frac{1}{2c^{2}} \left[\frac{\partial Q_{-}}{\partial t} + \frac{1}{2c^{2}} \left(\frac{\partial Q_{-}}{\partial t} + \boldsymbol{U} \cdot \nabla Q_{-} \right) \boldsymbol{U} \right] dS + \frac{1}{2c^{2}} \left[\frac{\partial Q_{-}}{\partial t} + \frac{1}{2c^{2}} \left(\frac{\partial Q_{-$$

or

$$\int_{V} \left[\frac{1}{2} |\nabla Q_{-}|^{2} + \frac{1}{2c^{2}} \left| \frac{DQ_{-}}{Dt} \right|^{2} - \frac{U \cdot \nabla Q_{-}}{c^{2}} \frac{DQ_{-}}{Dt} \right] dV = - \int_{0}^{t^{+}} \int_{S} \left[\frac{\partial Q_{-}}{\partial t} \frac{\partial Q_{-}}{\partial \bar{n}} - \frac{M_{n}}{c} \left| \frac{\partial Q_{-}}{\partial t} \right|^{2} \right] dS \tag{29}$$

where V represents the volume interior of S. The minus sign on the right hand side has been added due to the fact that the normal derivative used in the equation is still inward of the body surface. Note that, the left hand side of (29) is positive:

$$\begin{split} \int_{V} \left[\frac{1}{2} |\nabla Q_{-}|^{2} + \frac{1}{2c^{2}} \left| \frac{DQ_{-}}{Dt} \right|^{2} - \frac{U \cdot \nabla Q_{-}}{c^{2}} \frac{DQ_{-}}{Dt} \right] dV &= \frac{1}{2} \int_{V} \left[|\nabla Q_{-}|^{2} + \frac{1}{c^{2}} \left| \frac{DQ_{-}}{Dt} \right|^{2} - 2 \frac{U \cdot \nabla Q_{-}}{c^{2}} \frac{DQ_{-}}{Dt} \right] dV \\ &= \frac{1}{2} \int_{V} \left[\left(|\nabla Q_{-}| - \frac{1}{c} \left| \frac{DQ_{-}}{Dt} \right| \right)^{2} + 2 \frac{1}{c} |\nabla Q_{-}| \left| \frac{DQ_{-}}{Dt} \right| - 2 \frac{U \cdot \nabla Q_{-}}{c} \frac{DQ_{-}}{Dt} \right] dV \geq 0 \end{split}$$

for subsonic flows |U| < c. On the other hand, using (28), the right hand side of (29) will be negative:

$$-\int_0^{t^+} \int_S \left[\frac{\partial Q_-}{\partial t} \frac{\partial Q_-}{\partial \bar{n}} - \frac{M_n}{c} \left| \frac{\partial Q_-}{\partial t} \right|^2 \right] dS = \frac{1}{c^2} \int_0^{t^+} \int_S \left[\frac{a}{bc} \left| \frac{\partial Q_-}{\partial t} \right|^2 + \frac{M_n}{c} \left| \frac{\partial Q_-}{\partial t} \right|^2 \right] dS \le 0$$

provided

$$\frac{a}{b} < -\max(M_n) \tag{30}$$

The above implies that Q_{-} has to be a trivial solution,

$$Q_{-} \equiv 0$$

A simple choice for a and b is

$$a = -b = 1 \tag{31}$$

E. Comparison with earlier formulations

Extension of the Kirchhoff formula to a medium with a non-zero mean flow or to a static medium with moving surfaces have be studied extensively in the literature, both in the time domain and in the frequency domain. $^{16,17,39,51,53-56,58}$ In aeroacoustics studies, the most well-known formulations include those due to Ffowcs-Williams-Hawkings¹⁷ and Farassat-Myers. 16,55,56 These formulations were obtained through a use of generalized functions and have been widely used in noise predictions. The current formulation shown in (14) and (17), through the adjoint fundamental solution of the convective wave equation, is equivalent to those obtained by the generalized functions. A demonstration of the equivalence is offered below.

In [56], the pressure field by a moving surface by the Farassat-Myers method is expressed as

$$4\pi\phi H(f) = \int_{S} \frac{(M_n^2 - 1)\phi_n + M_n M_t \cdot \nabla_2 \phi + (1/c)E_1 \frac{\partial \phi}{\partial t} + (1/r)E_2 \phi}{r(1 - M_r)}|_{\tau^*} dS$$
 (32)

in which

$$E_1 = -M_n + \frac{\mathbf{n} \cdot \hat{\mathbf{r}} - M_n}{1 - M_r}, \quad E_2 = \frac{(\mathbf{n} \cdot \hat{\mathbf{r}} - M_n)(1 - M^2)}{(1 - M_r)^2}$$

Note that the equation above was developed in a static reference frame where the surface is moving, and the normal vector is assumed to be outward of the surface, opposite to the one used in the derivations in previous sections of this paper. We are going to show that equation (32) is equivalent to equation (14).

For convenience of discussion, let the receiver and source coordinates in the static frame be denoted as \tilde{r}' and \tilde{r} respectively. Then we have

$$\tilde{r} = r + \tau^* U, \quad \tilde{r}' = r' + t' U$$

where r and r' are the source and receiver locations in the moving frame. In (32),

$$r = |\tilde{r}' - \tilde{r}|, \text{ and } M_r = M \cdot \frac{\tilde{r}' - \tilde{r}}{|\tilde{r}' - \tilde{r}|}$$

It can be readily shown that⁵⁴

$$r(1 - M_r) = \bar{R}$$

where \bar{R} is as defined in (9). Furthermore, we have

$$\boldsymbol{n} \cdot \hat{\boldsymbol{r}} - M_n = \boldsymbol{n} \cdot \frac{\tilde{\boldsymbol{r}}' - \tilde{\boldsymbol{r}}}{|\tilde{\boldsymbol{r}}' - \tilde{\boldsymbol{r}}|} - M_n = \frac{\boldsymbol{n} \cdot [\boldsymbol{r}' - \boldsymbol{r} + (t' - \tau^*)\boldsymbol{U}]}{r} - M_n$$
$$= \frac{\boldsymbol{n} \cdot [\boldsymbol{r}' - \boldsymbol{r} + (r/c)\boldsymbol{U}]}{r} - M_n = \frac{\boldsymbol{n} \cdot (\boldsymbol{r}' - \boldsymbol{r})}{r}$$

where we have use the fact that

$$c(t' - \tau^*) = r$$

Then, when written in variables of the moving frame, equation (32) becomes

$$4\pi\phi H(f) = \int_{S} \frac{(M_{n}^{2} - 1)\phi_{n} + M_{n}M_{t} \cdot \nabla_{2}\phi + (1/c)\left(-M_{n} + \frac{\boldsymbol{n}\cdot(\boldsymbol{r}'-\boldsymbol{r})}{\bar{R}}\right)\frac{\partial\phi}{\partial t} + \frac{\boldsymbol{n}\cdot(\boldsymbol{r}'-\boldsymbol{r})}{\bar{R}^{2}}(1 - M^{2})\phi}{\bar{R}}\Big|_{\tau^{*}}dS$$

$$= \int_{S} \left[(M_{n}^{2} - 1)\frac{1}{\bar{R}}\phi_{n} + M_{n}\frac{1}{\bar{R}}M_{t} \cdot \nabla_{2}\phi + (1/c)\frac{1}{\bar{R}}\left(-M_{n} + \frac{\boldsymbol{n}\cdot(\boldsymbol{r}'-\boldsymbol{r})}{\bar{R}}\right)\frac{\partial\phi}{\partial t} + \frac{\boldsymbol{n}\cdot(\boldsymbol{r}'-\boldsymbol{r})}{\bar{R}^{3}}(1 - M^{2})\phi}\right]_{t_{R}'}dS \tag{33}$$

Equivalence to equation (14) follows immediately.

III. Time Domain Boundary Element Method

To solve the time domain boundary integral equation formulated in (24), a Boundary Element Method is used in this work. In this approach, the surface of the scatterer is discretized by a set of surface elements S_e :

$$S = \bigcup_{e=1}^{N_e} S_e$$

where N_e is the total number of elements. To facilitate the application of high-order basis functions, quadrilateral elements will be used. Each surface element is mapped to a standard element where collocation points based on the Chebychev-Gauss points are defined and local nodal basis functions are introduced, Figure 3. Integration over each element is carried out by high-order quadratures. However, no continuity is assumed across the element boundaries. In this way, boundary elements are completely unstructured and the order of the basis functions can be increased relatively easily.

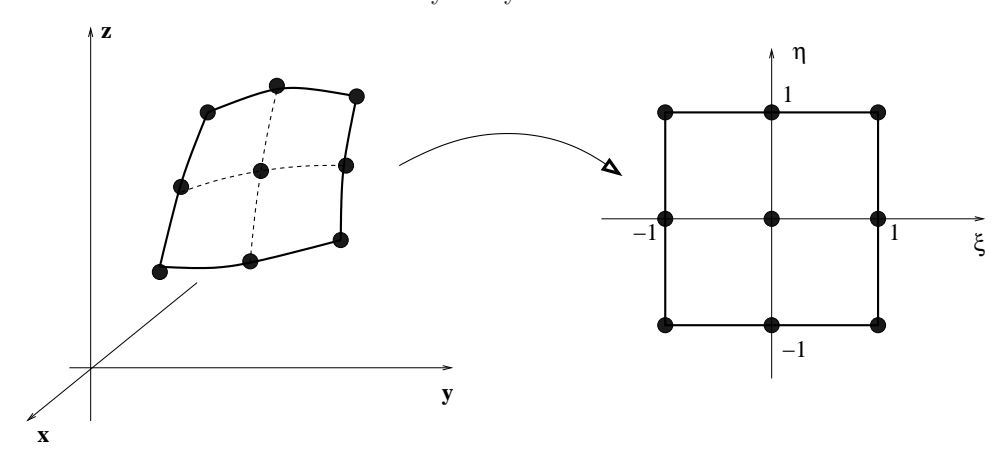


Figure 3. Mapping of a quadrilateral element to a standard domain in local variables (ξ, η) . Collocations points and high-order quadratures are based on the standard element.

Numerical solution on the surface is expressed as

$$p(\boldsymbol{r}_s, t) = \sum_{n=0}^{N_t} \sum_{i=1}^{N} u_i^n \phi_i(\boldsymbol{r}_s) \Psi(t - t_n)$$
(34)

in which $\phi_i(r_s)$ is the surface basis function for the ith node and $\Psi(\tau)$ is the temporal basis function defined as

$$\Psi(\tau) = \begin{cases}
\bar{\Psi}_0(\tau) & -\Delta t < \tau \le 0 \\
\bar{\Psi}_{-1}(\tau) & 0 < \tau \le \Delta t \\
\bar{\Psi}_{-2}(\tau) & \Delta t < \tau \le 2\Delta t \\
\bar{\Psi}_{-3}(\tau) & 2\Delta t < \tau \le 3\Delta t \\
0 & other
\end{cases} \tag{35}$$

where

$$\bar{\Psi}_{-\ell}(\tau) = \frac{\prod_{i=-3, i \neq \ell}^{0} [\tau + (i - \ell)\Delta t]}{\prod_{i=-3, i \neq \ell}^{0} [(i - \ell)\Delta t]}$$
(36)

Higher-order temporal basis functions can be similarly constructed. Basis functions with continuous derivatives have also been proposed recently.⁶⁹ The surface basis function $\phi_i(r_s)$ is a nodal polynomial constructed using Chebychev polynomials and is non-zero only on the element that contains node i. With these spatial and temporal basis functions, the expansion coefficient u_i^n in (34) represents the solution at ith node at time $t = t_n$.

By substituting expansion (34) into boundary integral equation (24), a March-On-in-Time scheme is obtained that is of the form

$$\mathbf{B}_0 \mathbf{u}^j = \mathbf{q}^j - \sum_{m=1}^{j_M} \mathbf{B}_m \mathbf{u}^{j-m} \tag{37}$$

where u^j denotes the vector of all unknowns u_i^j at time level t_j . Equation (37) relates the solution at time step $t = t_j$ to those at earlier time steps. The maximum time history required is dependent on the length of the scatterer and the mean flow as

$$j_{M} = \frac{\bar{L}}{c\alpha^{2}\Delta t}, \quad \bar{L} = \max_{\boldsymbol{r}_{s}, \boldsymbol{r}_{s}' \in S} \left[-\boldsymbol{M} \cdot (\boldsymbol{r}_{s} - \boldsymbol{r}_{s}') + \bar{R}(\boldsymbol{r}_{s}, \boldsymbol{r}_{s}') \right]$$
(38)

All the B_m matrices are sparse. In particular, we note that matrix B_0 in (37) is a very sparse matrix and represents interactions between nearby nodes at the same time level t_j . As a result, its inversion can be done easily by an iterative method, such as the Jacobi iterative method, with rapid convergence.³⁶

The computational challenge for the March-On-in-Time scheme of (37) lies in the computational cost associated with the evaluation of the right hand side of the equation. A direct evaluation of the right hand side of (37) has a computational cost at each time step of order $O(N^2)$ where N is the total number of nodes. This computational cost has to be reduced for the method to be useful for practical problems where N can be of order 10^6 or higher.

IV. Delay- and amplitude-compensated acoustic field in the presence of a mean flow

Fast multi-level and multi-grid time domain algorithms are used in this work to reduce the computational complexity for the evaluation of the right hand side of (24) and (37). A number of fast methods for time-domain wave equation have been proposed in the last decade. One is the multi-level Plane Wave Time Domain (PWTD) algorithm, ¹⁵ which is akin to the plane wave Fast Multipole Method (FMM) in the frequency domain. In this approach, using a Fourier representation integral and an extension from the frequency domain FMM, the time signals from a group of source points are combined and represented as outgoing plane waves, which are then translated and aggregated onto observer points. As a result, the contribution from a group of N_s source points to a group of M_s observer points, typically an order $O(N_s M_s)$ operation, can be reduced approximately to order $O(N_s) + O(M_s)$ operations, provided the time signal

is divided judiciously into small segments to satisfy causality. However, computation of the translation functions in PWTD is complicated due to the presence of ghost signals.

Another method for time domain March-On-in-Time acceleration is based on the observation that a specially constructed *delay- and amplitude-compensated* radiation field of a given group of sources can be represented by an extremely sparse and highly non-uniform space grid over the far-field.^{4,7,8} A recent Cartesian Non-uniform Grid Time Domain Algorithm (CNGTDA) has been given in [40, 47] exploiting the smoothness of the compensated field. This method will be used in the current study.

A. Derivation of delay- and amplitude-compensated field

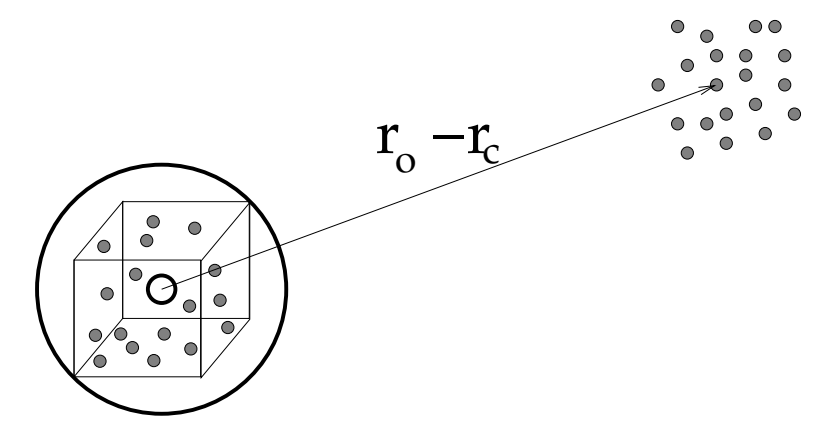


Figure 4. A diagram showing the group of source points, enclosed by a cubic box, and the far field receiver points. Due to the clustering of the source points, it becomes possible to get a spatially slow-varying far field when it is sampled at a characteristic time τ .

An extension of the delay- and amplitude-compensated acoustic field method from the simple wave equation to one with a nonzero mean flow has been carried out in the current work and will be used in this paper to accelerate the computation of the surface integrals in the time domain boundary integral equation (24).

Consider the acoustic field due to a group of N_s nodal points of source strength $q_i(t)$, located at $\mathbf{r}_i = (x_i, y_i, z_i)$ and within a sphere of radius R_s ,

$$p(\mathbf{r},t) = \sum_{i=1}^{N_s} \frac{q_i \left(t + \boldsymbol{\beta} \cdot (\mathbf{r} - \mathbf{r}_i) - \bar{R}(\mathbf{r}, \mathbf{r}_i) / c\alpha^2 \right)}{4\pi c^2 \bar{R}(\mathbf{r}, \mathbf{r}_i)}$$
(39)

where β , α and \bar{R} are as defined earlier. It is to be emphasized here that although point sources are used for this example, the analysis given below applies to other forms of sources, such as the discretized surface integral terms, in a straight forward manner.

The delay- and amplitude-compensated field at any point r for (39) is defined as

$$\tilde{p}(\boldsymbol{r},\tau) = \bar{R}_p(\boldsymbol{r},\boldsymbol{r}_c) \sum_{i=1}^{N_s} \frac{q_i \left(\tau + \boldsymbol{\beta} \cdot (\boldsymbol{r}_c - \boldsymbol{r}_i) + \tilde{R}_p(\boldsymbol{r},\boldsymbol{r}_c) / c\alpha^2 - \bar{R}(\boldsymbol{r},\boldsymbol{r}_i) / c\alpha^2 \right)}{4\pi c^2 \bar{R}(\boldsymbol{r},\boldsymbol{r}_i)}$$
(40)

where

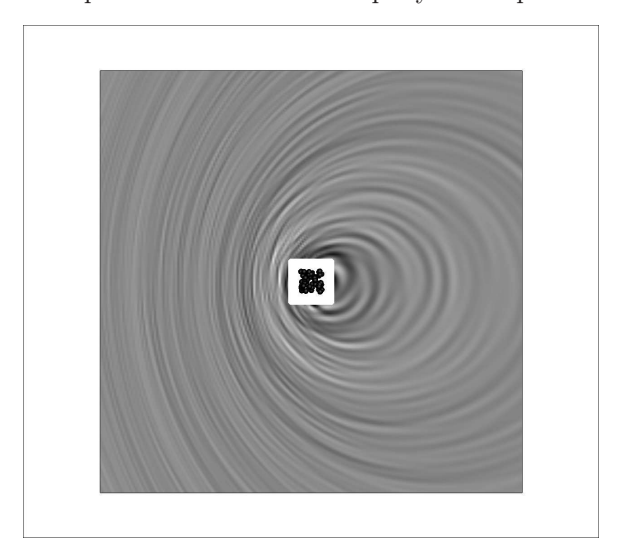
$$\bar{R}_p(r, r_c) = \sqrt{(x - x_c)^2 + \alpha^2 (y - y_c)^2 + \alpha^2 (z - z_c)^2}$$

$$\tilde{R}_{p}(\mathbf{r}, \mathbf{r}_{c}) = \sqrt{(x - x_{c})^{2} + \alpha^{2}(y - y_{c})^{2} + \alpha^{2}(z - z_{c})^{2} + L_{s}^{2}/2}$$

and
$$\tau = t + \boldsymbol{\beta} \cdot (\boldsymbol{r} - \boldsymbol{r}_c) - \tilde{R}_p(\boldsymbol{r}, \boldsymbol{r}_c)/c\alpha^2$$
 (41)

in which $r_c = (x_c, y_c, z_c)$ is the center of the sphere of radius R_s that contains the sources, as illustrated in Figure 4. The inclusion of the term with L_s is optional and its optimal value is to be determined later such that its use in \tilde{R}_p given in (41) provides the optimal delay compensation, as was argued in.^{4,7,8}

The advantage of using the delay- and amplitude-compensated field $\tilde{p}(\mathbf{r}, \tau)$ is that it can be represented by far fewer spatial points than those needed for the actual field $p(\mathbf{r}, t)$. As an illustration, Figure 5 shows an instantaneous acoustic field created by a group of 100 source points with random amplitudes and phases (left) and its delay- and amplitude-compensated field given by (40) (right). As demonstrated, spatial variation of the compensated field reduces rapidly as the points move away from the source region.



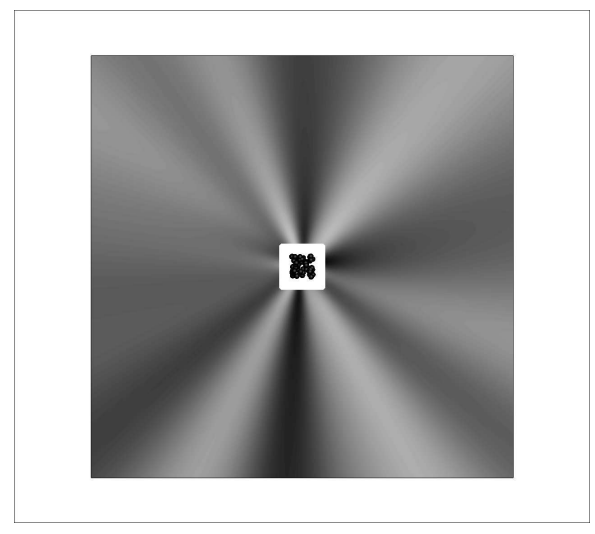


Figure 5. Left: An instantaneous acoustic field due to 100 random sources in a mean flow of Mach number 0.5; Right: The delay- and amplitude-compensated field of the same acoustic field at left.

For the field points far from the source box, instead of computing and storing $p(\mathbf{r},t)$, it is only necessary to compute and store $\tilde{p}(\mathbf{r},\tau)$ on a spatially coarse and highly non-uniform mesh. As a result, it requires a much smaller storage and fewer computations involving those nodal points on the interpolating mesh. Furthermore, the actual field due to the source points at any location and time (\mathbf{r},t) can be recovered by interpolating the compensated field,

$$p(\mathbf{r},t) = \frac{\tilde{p}(\mathbf{r},t + \boldsymbol{\beta} \cdot (\mathbf{r} - \mathbf{r}_c) - \tilde{R}_p(\mathbf{r},\mathbf{r}_c)/c\alpha^2)}{\bar{R}_p(\mathbf{r},\mathbf{r}_c)}$$
(42)

Hence, costs for computing interactions between nodal points can be greatly reduced by utilizing the compensated field. In particular, we note that once $\tilde{p}(\mathbf{r},\tau)$, or a representation of which, is obtained, computation of the actual field by (42) no longer requires the input of source points.

Note that the compensated field as given in (40) is computed on a time variable denoted by τ . Formulation of the compensated field is akin to a computation of solutions along the characteristics of the wave equation. The τ in (40) will be referred to as the *characteristics time*. A one-dimensional rendering of τ is shown in Figure 6.

To see the reason for the much reduced spatial variation of the compensated field $\tilde{p}(\mathbf{r},\tau)$, we consider the frequency domain expression for (40):

$$\tilde{p}(\mathbf{r},\omega) = \bar{R}_p \sum_{i=1}^{N_s} \frac{q_i(\omega)e^{-i\omega(\tau + \boldsymbol{\beta}\cdot(\mathbf{r}_c - \mathbf{r}_i) + \tilde{R}_p/c\alpha^2 - \bar{R}/c\alpha^2)}}{4\pi c^2 \bar{R}}$$
(43)

Note that, under a spherical coordinate $(x - x_c, \alpha(y - y_c), \alpha(z - z_c)) = (\rho \sin \phi \cos \theta, \rho \sin \phi \sin \theta, \rho \cos \phi)$,

$$\bar{R}^2 = \bar{R}_p^2 + \bar{R}_i^2 - 2\bar{R}_p\bar{R}_i\cos\phi$$

giving

$$\begin{split} \tilde{R}_{p} - \bar{R} &= \sqrt{\bar{R}_{p}^{2} + L_{s}^{2}/2} - \sqrt{\bar{R}_{p}^{2} + \bar{R}_{i}^{2}} - 2\bar{R}_{p}\bar{R}_{i}\cos\phi \\ &= \bar{R}_{p}\sqrt{1 + \frac{L_{s}^{2}}{2\bar{R}_{p}^{2}}} - \bar{R}_{p}\sqrt{1 + \frac{\bar{R}_{i}^{2}}{\bar{R}_{p}^{2}}} - 2\frac{\bar{R}_{i}}{\bar{R}_{p}}\cos\phi \\ \\ &= \bar{R}_{p}\left(1 + \frac{L_{s}^{2}}{4\bar{R}_{p}^{2}} + \cdots\right) - \bar{R}_{p}\left(1 + \frac{\bar{R}_{i}^{2}}{2\bar{R}_{p}^{2}} - \frac{\bar{R}_{i}}{\bar{R}_{p}}\cos\phi - \frac{1}{8}\left(\frac{\bar{R}_{i}^{2}}{\bar{R}_{p}^{2}} - 2\frac{\bar{R}_{i}}{\bar{R}_{p}}\cos\phi\right)^{2} + \cdots\right) \\ &= \bar{R}_{p}\left(1 + \frac{L_{s}^{2}}{4\bar{R}_{p}^{2}} + \cdots\right) - \bar{R}_{p}\left(1 + \frac{\bar{R}_{i}^{2}}{2\bar{R}_{p}^{2}} - \frac{\bar{R}_{i}}{\bar{R}_{p}}\cos\phi - \frac{1}{8}\left(4\frac{\bar{R}_{i}^{2}}{\bar{R}_{p}^{2}}\cos^{2}\phi + \cdots\right) + \cdots\right) \\ &= \bar{R}_{i}\cos\phi + \frac{1}{2\bar{R}_{p}}\left(\frac{L_{s}^{2}}{2} - \bar{R}_{i}^{2}(1 - \cos^{2}\phi)\right) + \cdots \end{split}$$

We see that the phase of the compensated field in (43) varies only with $O(\omega/\bar{R}_p)$, in contrast to $O(\omega\bar{R})$ for the actual field. Furthermore, the variation is minimized if

(44)

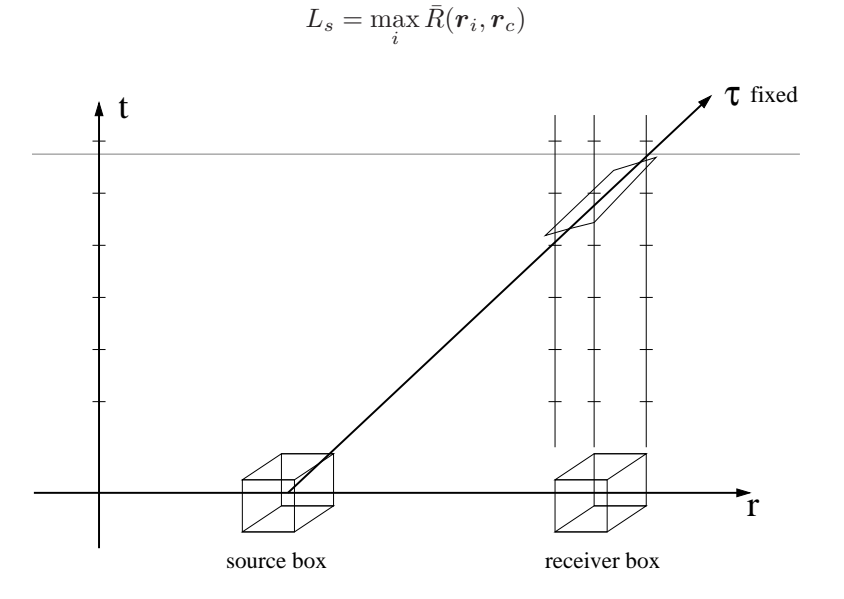


Figure 6. A diagram illustrating the characteristic time τ in a one-dimensionalized situation. The characteristic time represents the approximate propagation path for the sources in the group in this space-time diagram.

B. Multilevel implementation

Solution of the boundary integral equation is found in a time marching scheme (37) where at each time step the interactions between each element and every other elements as well as itself are computed. The interactions will be classified into *Near Interactions* and *Far Interactions*. Near interactions, where two elements are nearby, are computed directly. Far interactions, where elements are far apart (to be more precisely defined next), are computed using the compensated field.

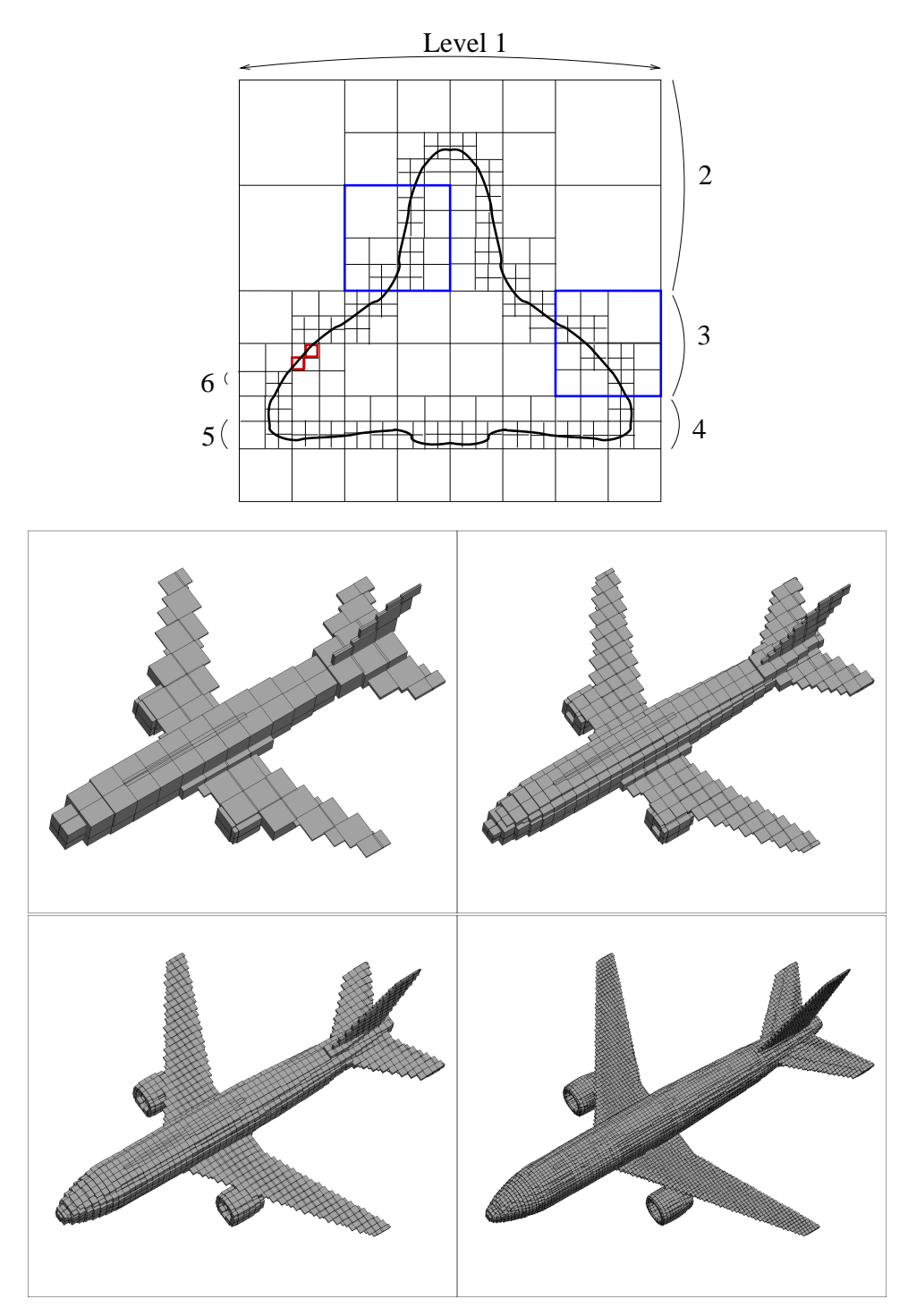


Figure 7. Surface elements are sub-divided into a hierarchy of boxes. Shown are the boxes for a conventional airplane at levels 5,6,7 and 8 with level 1 being the smallest box that encloses the entire airplane.

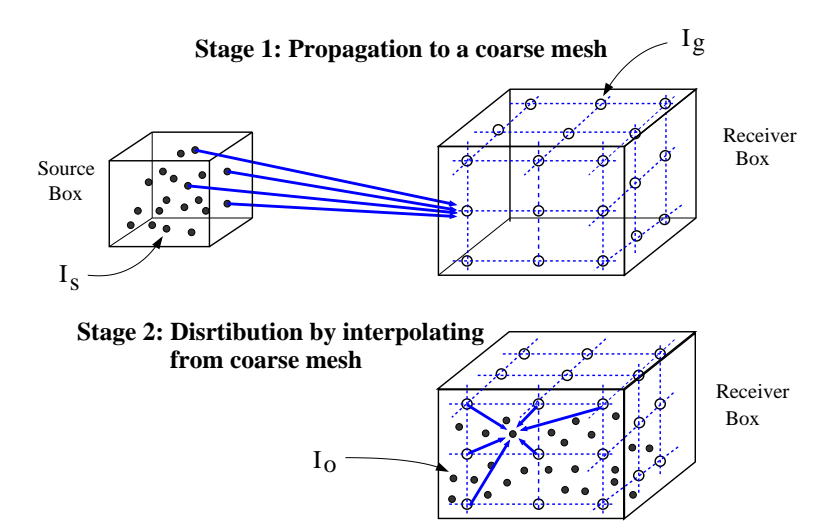


Figure 8. A schematic showing the two-stage approach for computing far interactions: Stage 1: the sources are propagated on to the interpolating mesh of the far field receiver box; Stage 2: the actual field values on the elements within the receiver box are interpolated from the interpolating mesh. These two steps are referred to as the Propagation-Distribution scheme.

To facilitate the application of the delay- and amplitude-compensated field to the solution of the boundary integral equation (24), an oct-tree box hierarchy is constructed by successively dividing the box that bounds the body of surfaces, from level $\ell=1$ (highest) to $\ell=L$ (lowest), a schematic in 2D is shown in Figure 9. An interaction list is created where any box pair that satisfies the following conditions, and any of their parents does not, is treated as far interactions:

$$\bar{R}_c > \bar{R}_{min}(B_s, B_o)$$
 (Causality)
 $\bar{R}_s/\lambda_{min} < \gamma$ (Accuracy)

$$N_s > n_{min}$$
 (Efficiency)

in which γ is a ratio for accuracy and n_{min} is the minimum number of elements within a box for far interaction to be cost effective. Here \bar{R}_c denotes the distance between the centers of source and receiver boxes and \bar{R}_{min} denotes the minimum requirement for far interaction condition (to be defined later). For far interactions, a two-step strategy will be implemented. In the first step, the compensated field of each source box is computed at a coarse interpolating mesh in each receiver box. In the second step, the actual field values on each receiver element are interpolated from the compensated field values of the interpolating mesh that they belong. This is as illustrated in Figure 8. These two steps will be referred to as Propagation and Distribution respectively.

C. Time Domain Propagation and Distribution Algorithm

Consider a far interaction between a source box B_s and a receiver box B_o . The interaction will be computed in two stages. In the first stage, solutions on all the source nodes within B_s are propagated to a coarse interpolating grid of the observer/receiver box using compensated field. In the second stage, the compensated field on each observer element is computed by interpolation from those of the coarse grid and immediately distributed to the actual time grid by anterpolation. Details on the implementation of these two steps are given below.

Let I_s denote the set of all source points in the source box B_s , and I_g and I_o denote the sets of interpolating grid and the receiver nodes in the receiver box B_o respectively. The essential steps for the far interactions using the Time Domain Propagation and Distribution Algorithm (TDPD) are as follows:

1. Assume complete solutions are available for $t \leq t_j$. At time $t = t_j = j\Delta t$, determine τ_j such that

$$\tau_j + \frac{\tilde{R}_p(\boldsymbol{r}_o, \boldsymbol{r}_c)}{c\alpha^2} - \beta(x_o - x_c) \ge t_j \tag{45}$$

for all grid points and nodal points \mathbf{r}_o in receiver box B_o . This leads to the choice of

$$\tau_j = t_j - \min_{\boldsymbol{r}_o \in I_g, I_o} \left[\frac{\tilde{R}_p(\boldsymbol{r}_o, \boldsymbol{r}_c)}{c\alpha^2} - \beta(x_o - x_c) \right]$$
(46)

2. Compute compensated field on the coarse interpolating grid $\mathbf{r}_o^{I_g}$ as follows,

$$\tilde{p}(\boldsymbol{r}_{o}^{I_{g}}, \tau_{j}) = \bar{R}_{p}(\boldsymbol{r}_{o}^{I_{g}}, \boldsymbol{r}_{s}^{i}) \sum_{i=1}^{N_{s}} \frac{q_{i}(\tau_{j} + \boldsymbol{\beta} \cdot (\boldsymbol{r}_{c} - \boldsymbol{r}_{s}^{i}) + \tilde{R}_{p}(\boldsymbol{r}_{o}^{I_{g}}, \boldsymbol{r}_{c})/c\alpha^{2} - \bar{R}(\boldsymbol{r}_{o}^{I_{g}}, \boldsymbol{r}_{s}^{i})/c\alpha^{2})}{4\pi c^{2}\bar{R}(\boldsymbol{r}_{o}^{I_{g}}, \boldsymbol{r}_{s}^{i})}$$

$$(47)$$

Note that causality at the source points requires that

$$\tau_j + \boldsymbol{\beta} \cdot (\boldsymbol{r}_c - \boldsymbol{r}_s^i) + \tilde{R}_p(\boldsymbol{r}_o, \boldsymbol{r}_c)/c\alpha^2 - \bar{R}(\boldsymbol{r}_o, \boldsymbol{r}_s^i)/c\alpha^2 \le t_j$$
(48)

which leads to the condition on the source and receiver boxes,

$$\max_{\boldsymbol{r}_s^i \in B_s, \boldsymbol{r}_o \in B_o} \left[\beta(x_c - x_s^i) + \frac{\tilde{R}_p(\boldsymbol{r}_o, \boldsymbol{r}_c)}{c\alpha^2} - \frac{\overline{R}(\boldsymbol{r}_o, \boldsymbol{r}_s^i)}{c\alpha^2} \right] \le \min_{\boldsymbol{r}_o \in B_o} \left[\frac{\tilde{R}_p(\boldsymbol{r}_o, \boldsymbol{r}_c)}{c\alpha^2} - \beta(x_o - x_c) \right]$$

This condition is approximately the following on the distance between the centers of the boxes:

$$\bar{R}_{c} \geq \max_{\boldsymbol{r}_{o} \in B_{o}} \left[\tilde{R}_{p}(\boldsymbol{r}_{o}, \boldsymbol{r}_{c}) \right] - \min_{\boldsymbol{r}_{o} \in B_{o}} \left[\tilde{R}_{p}(\boldsymbol{r}_{o}, \boldsymbol{r}_{c}) \right] + \max_{\boldsymbol{r}_{s}^{i} \in B_{s}, \boldsymbol{r}_{o} \in B_{o}} \left[\bar{R}_{c} - \overline{R}(\boldsymbol{r}_{o}, \boldsymbol{r}_{s}^{i}) \right] + |\boldsymbol{M}| \frac{L_{x}}{2} + \max_{\boldsymbol{r}_{o} \in B_{o}} \left[M(x_{o} - x_{c}) \right]$$

$$(49)$$

where L_x is the maximum dimension of the source box in x.

- 3. By interpolating spatially, get the compensated field at each observation point $\tilde{p}(\mathbf{r}_o^{I_o}, \tau_j)$ from those at the interpolating grid $\tilde{p}(\mathbf{r}_o^{I_g}, \tau_j)$
- 4. Recover actual field $p(\mathbf{r}_o^{I_o}, t')$ at time $t' = \tau_j + \frac{\tilde{R}_p(\mathbf{r}_o^{I_o}, \mathbf{r}_c)}{c\alpha^2} \boldsymbol{\beta} \cdot (\mathbf{r}_o^{I_o} \mathbf{r}_c)$ by

$$p(\mathbf{r}_o^{I_o}, t') = \frac{\tilde{p}(\mathbf{r}_o^{I_o}, \tau_j)}{\bar{R}_p(\mathbf{r}_o^{I_o}, \mathbf{r}_c)}$$

$$(50)$$

5. Distribute $p(\mathbf{r}_{o}^{I_{o}}, t')$ to $p(\mathbf{r}_{o}^{I_{o}}, t_{k})$, $p(\mathbf{r}_{o}^{I_{o}}, t_{k+1})$, $p(\mathbf{r}_{o}^{I_{o}}, t_{k+2})$ and $p(\mathbf{r}_{o}^{I_{o}}, t_{k+3})$ by anterpolation, where

$$k = \left[\frac{t'}{\Delta t} \right]_{floor} = \left[\frac{1}{\Delta t} \left[\tau_j + \frac{\tilde{R}_p(\boldsymbol{r}_o^{I_o}, \boldsymbol{r}_c)}{c\alpha^2} - \boldsymbol{\beta} \cdot (\boldsymbol{r}_o^{I_o} - \boldsymbol{r}_c) \right] \right]_{floor}$$
(51)

and

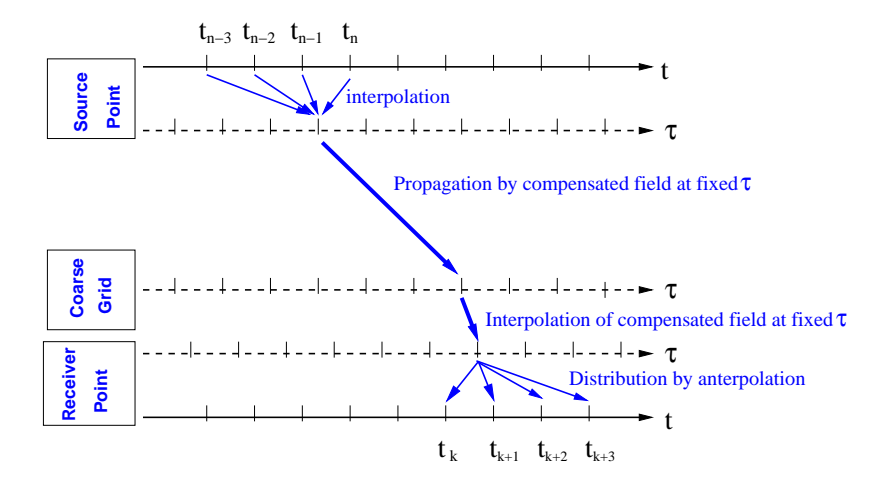


Figure 9. An illustration of interpolation and anterpolation for the time grids at source and receiver boxes. Values of the compensated field on the characteristics time grid τ is distributed onto the real time grid. Far field values are aggregated automatically and stored on real time t grid.

$$p(\mathbf{r}_{o}^{I_{o}}, t_{k+\ell}) = p(\mathbf{r}_{o}^{I_{o}}, t_{k+\ell}) + \Psi(t_{k+\ell} - t')p(\mathbf{r}_{o}^{I_{o}}, t'), \ \ell = 0, 1, 2, 3$$
(52)

The above algorithm gives a complete description for propagating a time signal from a cluster of source points to a group of far receiver points contained in a far interaction box.

We note that the compensated field is to be constructed in the characteristics time τ , whose grid usually will not coincide with that of the real time t. The values at the source locations required for (47) can be obtained by interpolation. If the same temporal basis functions as (35) are used, we have, for any given t,

$$q(\mathbf{r},t) = q(\mathbf{r},t_n)\Psi(t-t_n) + q(\mathbf{r},t_{n-1})\Psi(t-t_{n-1}) + q(\mathbf{r},t_{n-2})\Psi(t-t_{n-2}) + q(\mathbf{r},t_{n-3})\Psi(t-t_{n-3})$$
(53)

where

$$n = \left\lceil \frac{t}{\Delta t} \right\rceil_{ceiling}$$

On the observer mesh I_g , given the values on the characteristics time τ , the actual field on the real t time grid may also be similarly interpolated from the τ grid, as is done in [47]. However, doing so will result in a storage of time history on the τ grid and separate storage for each source box on the same receiver and excessive interpolation operations. A more efficient treatment is to distribute $p(\mathbf{r},t')$ onto the t time grid as follows: any value of $p(\mathbf{r},\tau)$ on the characteristics time grid is distributed to the t grid as soon as it is computed, eliminating the need for storing the time history of $\tilde{p}(\mathbf{r}_o^{I_g},\tau_j)$ and $p(\mathbf{r}_o^{I_o},t')$. In other words, $p(\mathbf{r},\tau)$ is distributed to $p(\mathbf{r},t_k)$, $p(\mathbf{r},t_{k+1})$, $p(\mathbf{r},t_{k+2})$ and $p(\mathbf{r},t_{k+3})$ with weights $\psi(t_k-t')$, $\psi(t_{k+1}-t')$, $\psi(t_{k+2}-t')$ and $\psi(t_{k+3}-t')$ respectively, where k is as defined in (51), as illustrated in Figure 9. This distribution is also referred to as anterpolation. Aggregation of contributions from all source boxes is done automatically through (52).

Compared to the CNGTDA in [47], the interaction list in the present algorithm is not limited to the boxes in the same level. This is computationally more efficient in the time domain because the interpolation to the characteristics time at each source box needs to be done only once per time step.

In Figure 10, the signal for the right hand side of (24) due to a group of randomly phased source elements is plotted, together with the signal obtained by direct evaluation of the integrals. Very good agreements are shown.

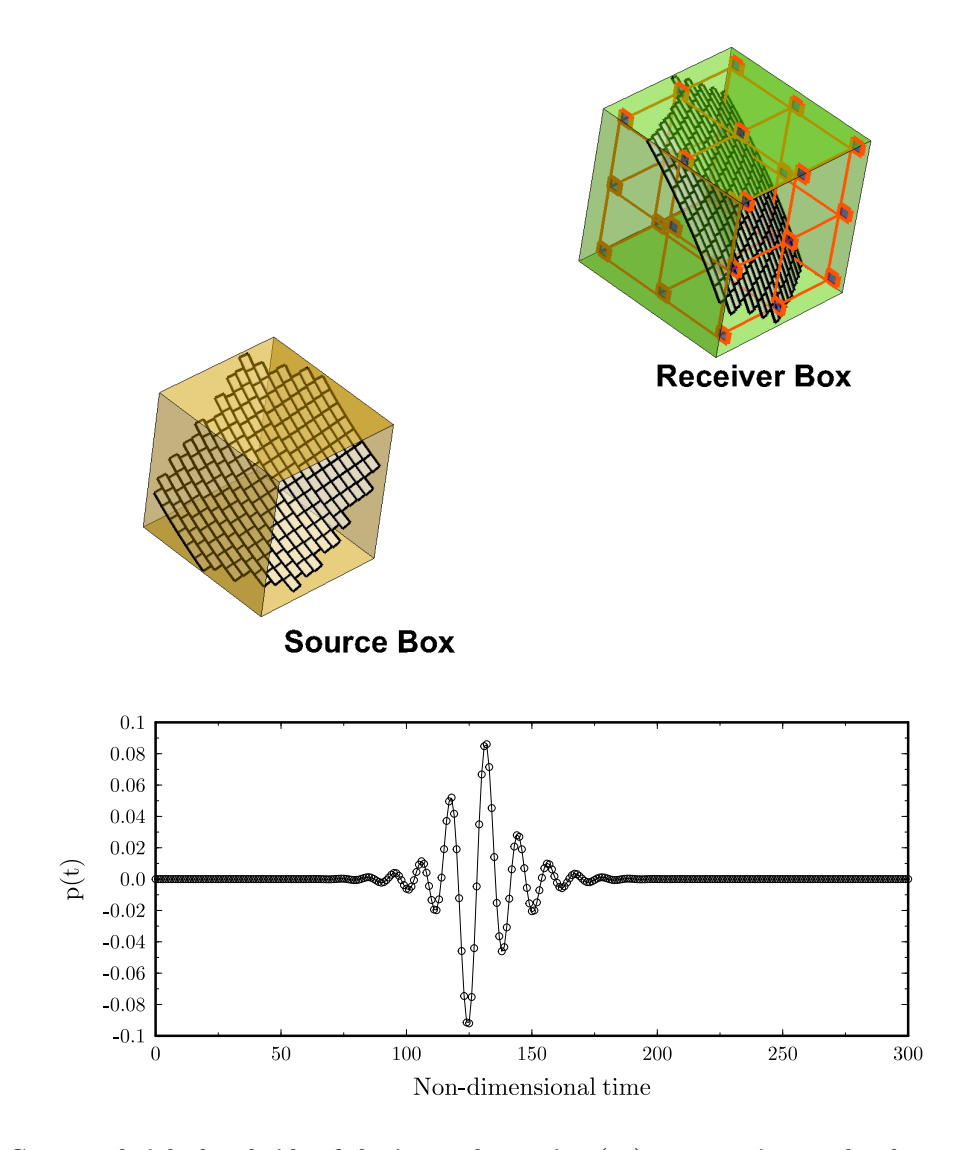
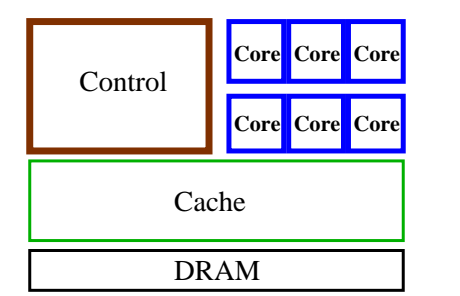


Figure 10. Computed right hand side of the integral equation (24) on a receiver nodes due to all the source nodes in the source box, mean flow Mach number M=0.2. Over 200 elements are included in each of the source and receiver boxes. Only a 3x3 interpolating mesh of Chebychev-Gauss points is used. Line: computed by the Time Domain Propagation and Distribution Algorithm; Symbol: computed directly.

V. GPU acceleration

GPU (Graphics Processing Unit) computing is a recently emerged alternative for High Performance Computing. General Purpose GPU (GPGPU) computing is a technology that is rapidly evolving. Unlike CPUs, GPUs have a throughput-oriented architecture. ^{18,21} A GPU contains many microprocessors (MP) and each microprocessor can execute a massive number of threads on streaming processor (SP) cores. It employs SIMD (Single Instruction Multiple Data) data processing model. For instances, for the NVIDIA C2090 model (FERMI architecture), a single GPU has 512 cores, and the most recent product Tesla K20 has 2496 cores and delivers over one Teraflops in double precision. A comparison between CPU and GPU architectures is illustrated in Figure 10. Programming on GPU has been made considerably simpler with the releases of CUDA (Compute unified device architecture)⁵⁷ and OpenCL (Open Computing Language)⁶⁸ programming tools.



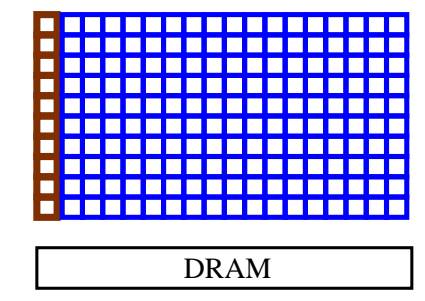


Figure 11. A schematic of comparison between CPU and GPU archtectures. While CPUs have a sophisticated cache structure, GPU are designed to have massively large number of computing cores.

Research papers on GPU for scientific computing have appeared in recent literature. Orders-of-magnitude speed-ups over a single CPU performance have been achieved in a diverse field of applications, including finite element methods, finite difference methods, integral equation methods and multi-body problems. ^{29, 37, 38, 40, 41, 67} GPU computing is fast becoming a new research area in high performance computing.

GPU computing favors intrinsically parallel algorithms. It is most effective when a time consuming computation can be efficiently divided into independent small computations. Such massive parallelism is naturally abundant in the time domain Boundary Element Methods. At each time step, computations on each element can be carried out independently, resulting in a high degree of parallelism. This makes the time domain BEM a good application for GPU computing.

GPU computing has been integrated to accelerate the present algorithm in two ways. First, for near-field interactions, high degree of parallelization can be realized as each element requires only information from its close neighbors within a distance of a few time steps of propagation. Especially, on singular elements where the source and observer points are on the same element, high-order integration quadratures are usually needed to treat the singular or hypersingular integration. These interactions are localized and computing intensive, ideal for GPU execution. The near-filed interaction coefficients can be computed by GPU on the fly to reduce memory requirement.

Second, for far-field interactions, the construction of compensated field for each source box outlined in propagation stage can also be carried out independently. As such, one thread block can be assigned to each element in a source box, where the memory can be shared among the threads in the block.

In Cuda Fortran, GPU computing is carried out through user defined functions called *kernels*. A kernel function is to be executed, by design, on a specified grid of threads. All threads, in the tens of thousands, are executed concurrently. Accordingly, in the solution of time domain boundary element method, two kernel functions are created, one for the near interactions and the other for the far interactions. The dimensions of threads are further sub-divided into blocks. Use of shared memory within each block speeds up memory access dramatically. In Figure 12, a GPU computing grid formed by source elements and receiver elements is illustrated, where one source element fits one block, and one GPU computing thread is assigned for a single interaction between a quadrature point and a receiver node.

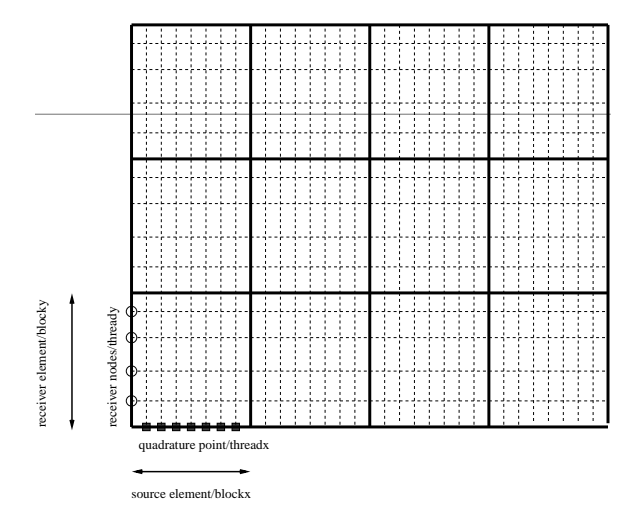


Figure 12. A schematic of a GPU computing grid. Each grid point represents an indexed computing thread. The threads are further organized into blocks where shared memory is allocated and available for all threads within the block.

Number of unknowns	3 GPUs	3 CPU cores	30 CPU cores	60 CPU cores	120 CPU cores
	(M2090)	(XEON 2.8Ghz)			
8100	2.10	65.03 (31)	6.65 (31)	4.12 (39)	3.62 (68)
32459	15.38	510.18 (33)	58.85 (38)	29.15 (38)	21.65 (56)
72925	42.21	1381.41 (33)	144.14 (34)	83.83 (40)	63.67 (60)

Table 1. Computational time (Wall Clock) per time step in seconds, in GPU and CPU with indicated number of cores. Number in parenthesis indicates the pro-rated speedup of GPU v.s. per CPU core.

In Table I, a comparison between the GPU and CPU execution time is given. Compared to a single CPU core, use of one GPU gains a speedup of over 30 times. While a modern CPU open has multiple cores, 12 or more, the table also shows that inter-nodal communications can slow down the computation significantly. Use of GPU can effectively reduce the communication time. The GPU as an computing accelerator has a particularly strong impact on a single-workstation computing environment.

VI. Sample results

In this section, sample results of time domain scattering computations are shown. All computations were carried out in the time domain and the frequency domain solutions were obtained by post processing. All sources in the examples are modeled as point sources initiated with a broadband pulse of short duration. The time function q(t) for sources used in the examples is as follows:³²

$$q(t) = \frac{\Delta t \sin(\omega_0 t)}{\pi t} e^{(\ln 0.01)(t/M\Delta t)^2}, \quad |t| \le M\Delta t$$
 (54)

where $\omega_0 \Delta t = \pi/5$, M = 50.

For a few pre-selected frequencies, the frequency domain solution can be computed concurrently with the time domain solution,

$$p(\mathbf{r},\omega) = \Delta t \left[p(\mathbf{r},t_1)e^{-i\omega t_1} + p(\mathbf{r},t_2)e^{-i\omega t_2} + p(\mathbf{r},t_3)e^{-i\omega t_3} + \cdots \right]$$
(55)

The advantage of this method is that the frequency domain solutions at these frequencies become immediately available at the end of time marching and no storage for the time history is needed. The disadvantage is that the computational cost increase rapidly when the number of required frequencies increases. Another option to get the frequency domain solution is to carry out an FFT of the time domain solution. Computationally, the second option would be more efficient when a large number of frequencies are of interest.

A. Point source scattering by a sphere

In this example, scattering of a point source by a sphere is computed to demonstrate the time domain solution and its frequency domain results. In Figure 13 (top), and instantaneous contour plot is shown as the point source with a time function specified in (54) is reflected by the sphere. The frequency domain solutions, obtained though (55) are also shown in Figure 13.

A comparison with the exact solution is shown in Figure 14. We note that solutions of all frequencies within the numerical resolution are available in the same time domain simulation. Comparisons in L2 norms are shown in Figure 15 for varying total number of elements. The absolute values of the solutions are used in the comparison. The relative error in L2 norm reduces with the increase in the number of surface elements.

B. Scattering by an airplane

In this example, scattering of two point sources placed above the airplane wings is computed. The purpose of the example is to demonstrate the application of the time domain boundary element method to problems with a compex geometry and at high frequencies. The geometry in the example is from the NASA Common Research Model²⁰ with a total of 1,314,144 qudrilateral elements on the surface of the airplane. The elements are organized into an oct-tree of 10 levels. An interaction list for far interactions is created and acounts for over 99.5% of the all interactions. Computation is carried out on a cluster of 72 GPUs (NVIDIA M2090) in less than 24 hours. After the time domain simulation is done, the frequency domain solution are available at any frequency within the numerical resolution. Frequency domain solutions at a few selected frequencies obtained by (55) are shown in Figure 16.

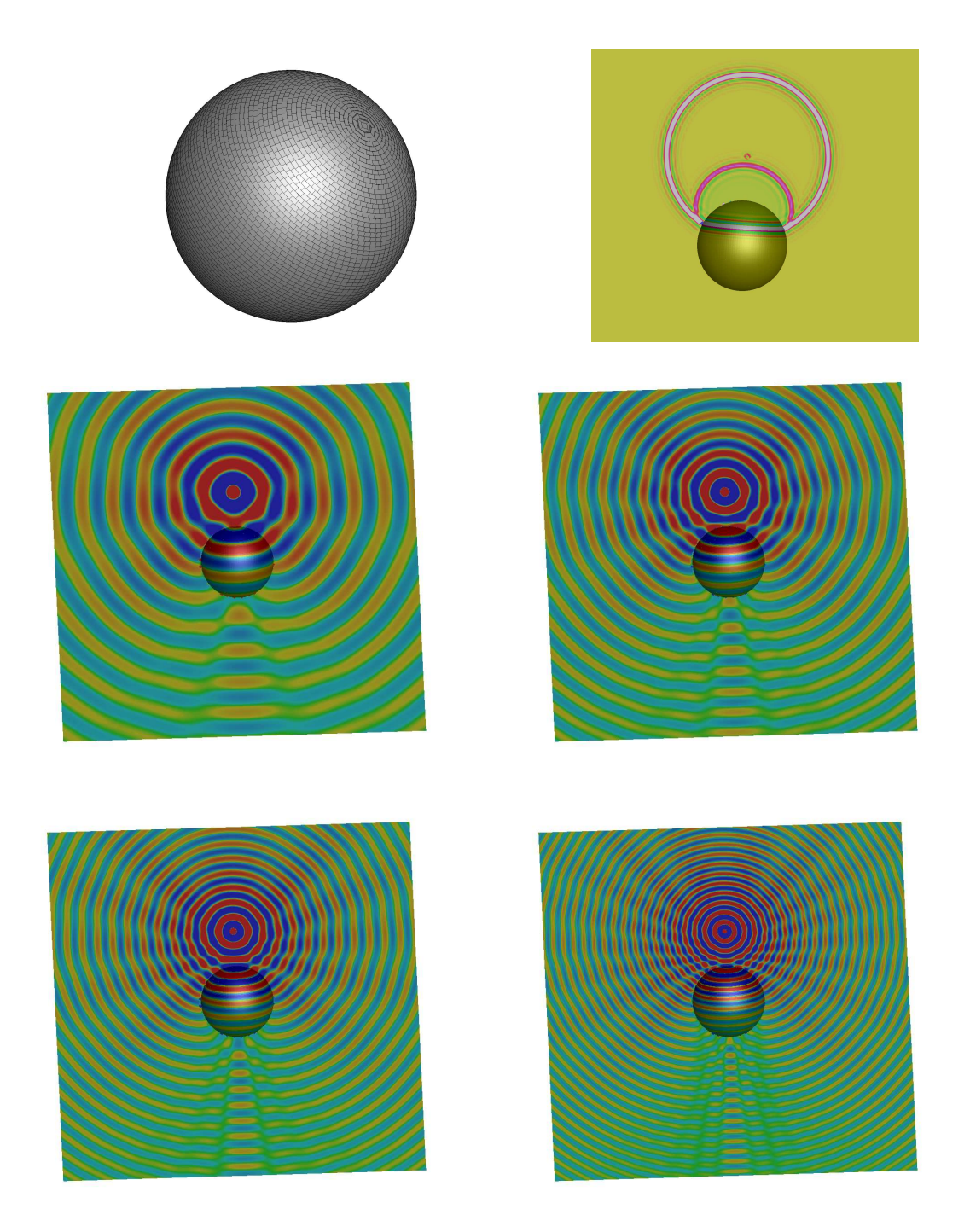


Figure 13. Scattering of a point source by a sphere. Top figure is an instantaneous contour plot. Frequency domain solutions at $\omega a/c=2\pi, 3\pi, 4\pi, 6\pi$ are shown.

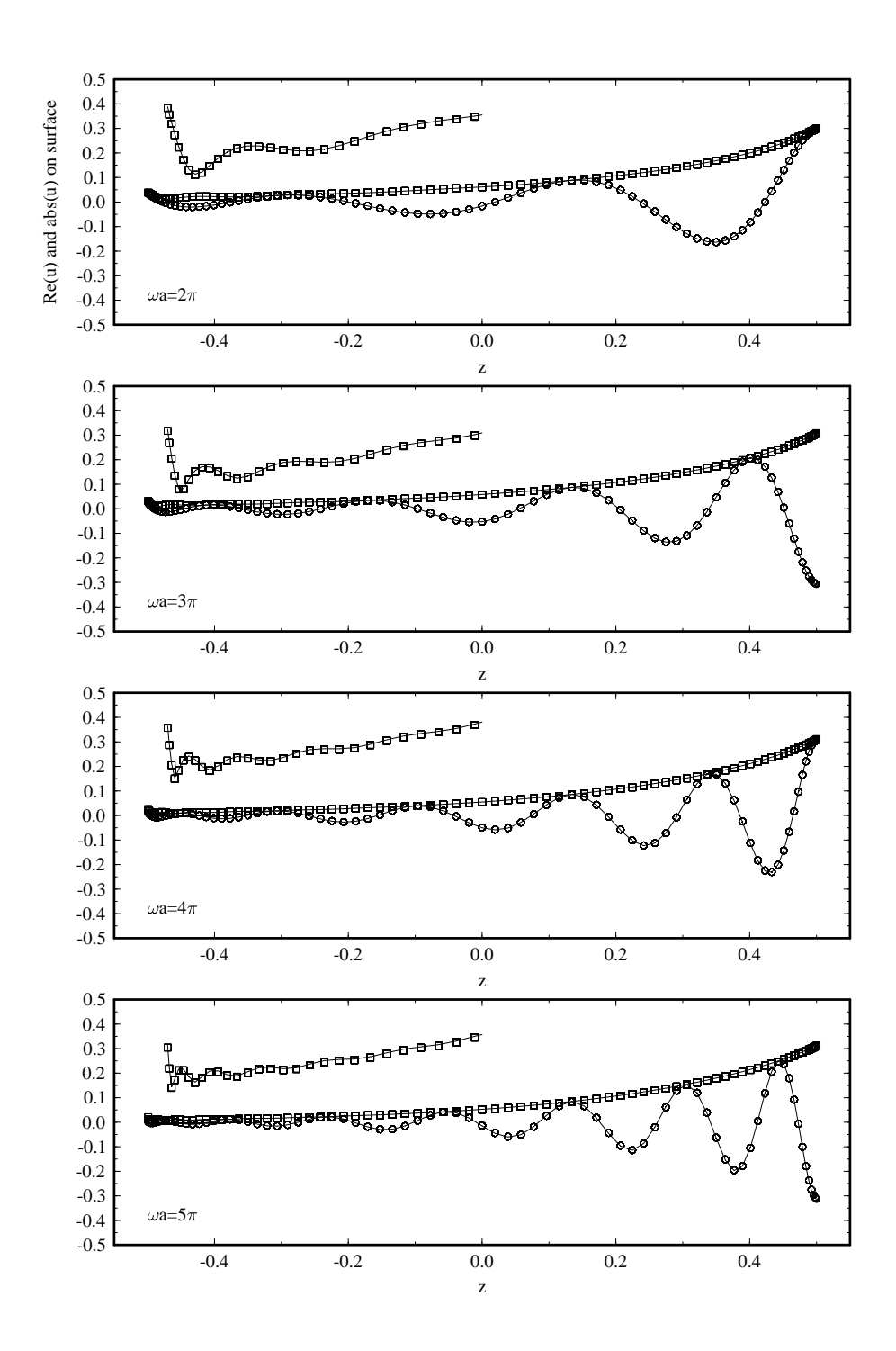


Figure 14. Comparison of numerical (symbols) and exact (line) solutions for $p(z,\omega)$ on the surface of the sphere. Square: absolute values; circle: real part. Also shown in inserts are the magnified solutions at the shadow region. The radius of sphere is a=0.5 and the source point is located at (0,0,1). A total of 5200 constant elements are used on the surface of the sphere.

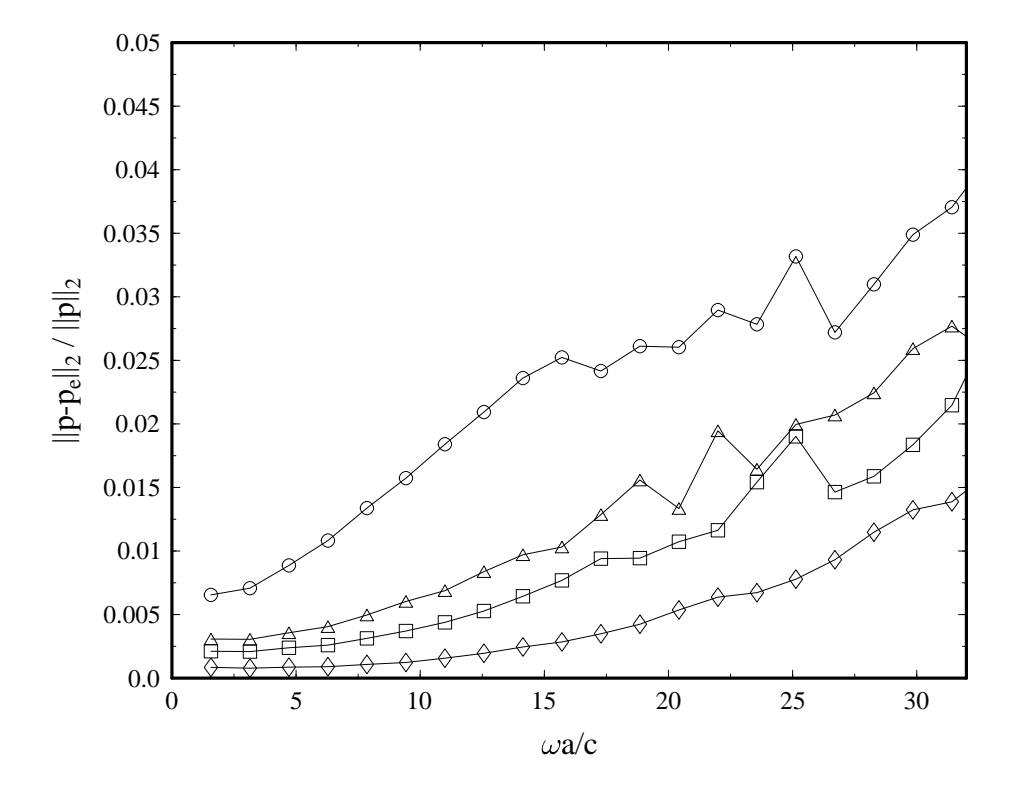


Figure 15. Relative L2 norm of the differences between the numerical and exact solutions (absolute values). Constant elements are used. \circ : N = 2050; \triangle : N = 5200; \square : N = 8100; \diamondsuit : N = 32459.

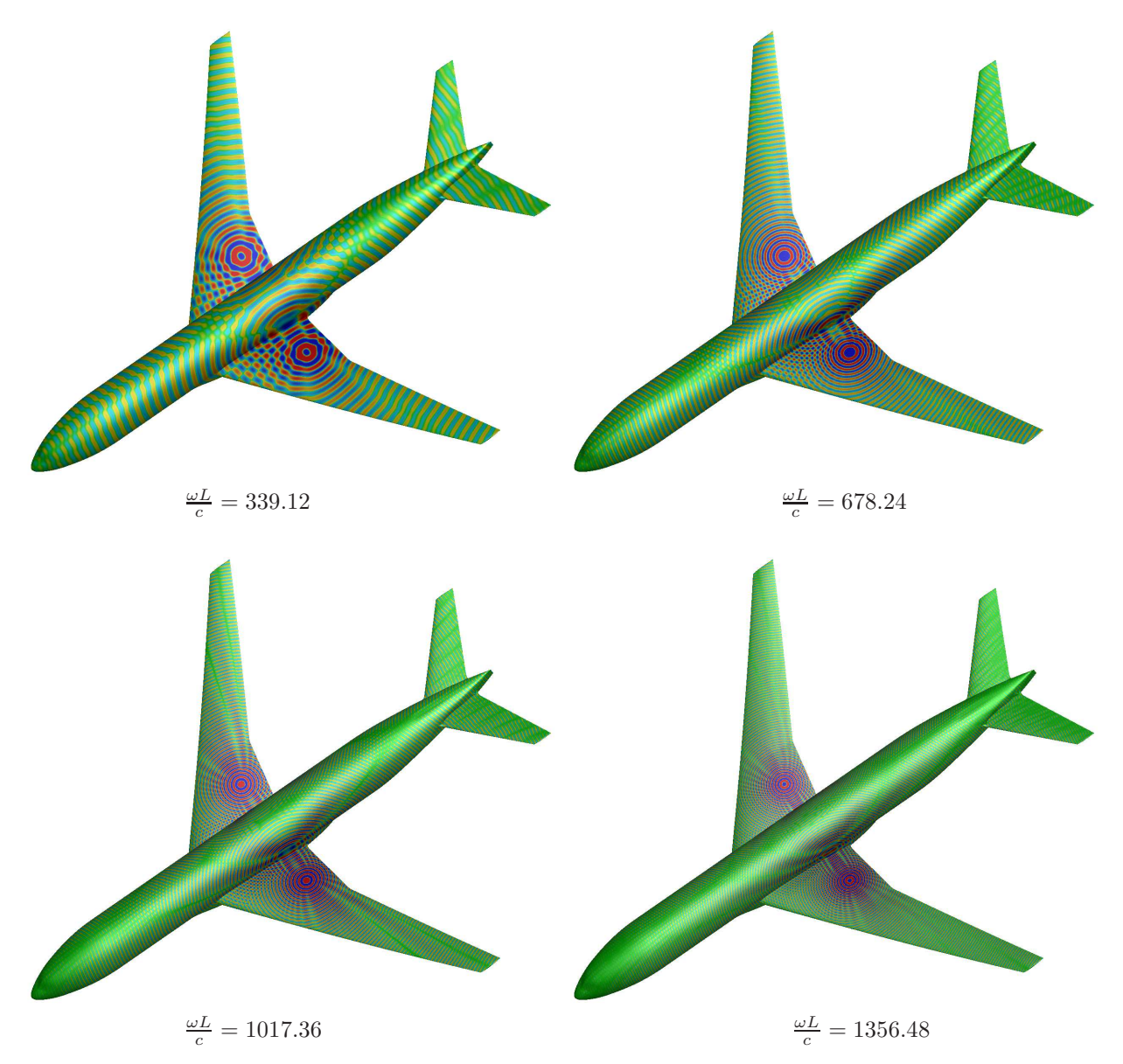


Figure 16. Frequency domain solution of scattering by an airplane at selected frequencies. The geometry is from the NASA Common Research Model with 1,354,144 surface elements. Constant elements have been used for the computation.

An operation count has been conducted for the Common Research Model airplane as the number of total surface elements increases. The trends for the increase of the operations for far interactions and near interactions per time step are shown in Figure 17. With an increase in the oct-tree levels along with the increase in the total number of elements, computational cost for the near interaction can be kept to grow linearly with N as expected. The cost for far interactions, for both the propagation and distribution stages, increases as $N^{1.25}$. However, we note that the cost for the distribution stage is much lower than that of the propagation stage, due to the fact that a high-order quadrature has been used for evaluation of the surface integrals on the element, where number of quadrature points far exceeds the number of collocation points.

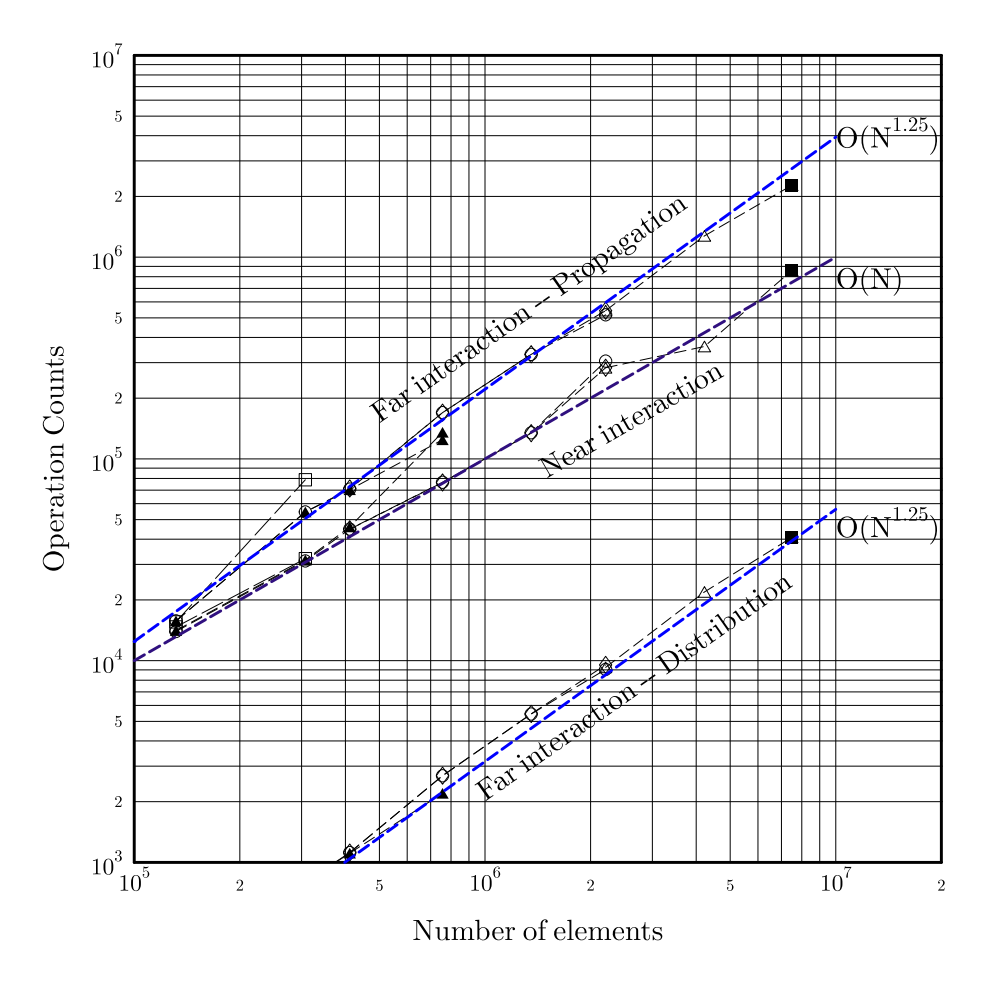


Figure 17. Operational count (in 10^9) as a function of total number of elements. Trend lines are as shown. Symbols indicate the total elvels in the oct-tree structure, \Box : 7 levels; \blacktriangle : 8 levels; \diamond : 9 levels; \diamondsuit : 10 levels; \blacktriangle : 11 levels; \blacksquare : 12 levels.

C. Solution with far field signatures

In this example, far field solutions are computed in addition to the solution on the surface of the airplane. Once the solution on the surface of the scatterer is found, field values can be obtained by (14) or (24). The frequency domain solutions are shown in Figure 18. For this example, the mean flow Mach number M = 0.2.

VII. Conclusions

Numerical solution of the time domain boundary integral equation (TDBIE) for convective wave equation with a non-zero mean flow has been considered in this paper. An extended Kirchhoff formula has been

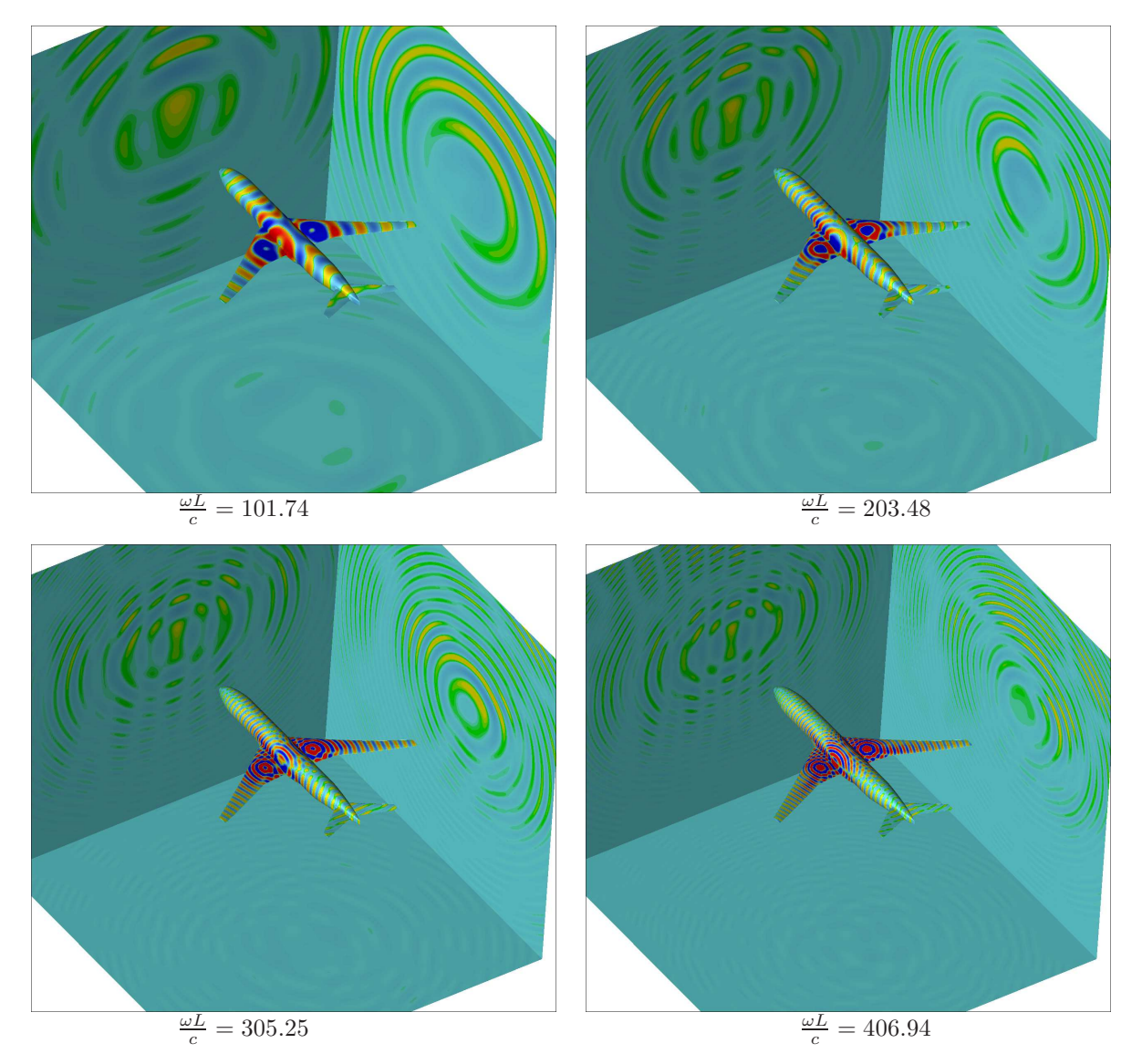


Figure 18. Frequency domain solution with the far field signature. Also shown are the surface mesh and the mesh for far field data. Flow Mach number M=0.2 with 131,553 elements on airplane surface.

presented and the implied boundary integral equation that relates the pressure and its normal derivative at the boundary has been derived. For numerical solution of the exterior scattering problem, a stable Burton-Miller type formulation has been proposed where the resonance frequencies in the interior domain are eliminated. Numerical experiements suggest that the formulation is stable for time domain boundary element methods.

To significantly reduce the computational cost of the time domain Boundary Element Method (TDBEM), a Time Domain Propagation and Distribution (TDPD) algorithm has been developed, based on the delay-and amplitude-compensated field and the recently proposed multi-level Cartesian Non-uniform Grid Time Domain algorithm (CNGTDA). The computational cost can be reduce from $O(N^2)$ to $O(N^{1.25})$, making it a potentially practical approach for computing scattering solution with millions of surface elements in time domain under currently available computational capabilities.

The recently emerged General Purpose GPU (GPGPU) computing has also been utilized to speed up the computation. A speed up of 30 times has been observed for the current algorithm comparing the performances on a single GPU (M2090) and a single CPU core (XEON 2.8GHz). As such, use of GPU can accelerate the computation dramatically especially in a single workstation environment. The speedup also results in a need of fewer computational nodes and thus reduces inter-nodal communication cost.

Acknowledgements

This work is supported by a NASA Coorperative Agreement, NNX11AI63A. The technical monitor is Dr. Douglas M. Nark. This work used the Extreme Science and Engineering Discovery Environment (XSEDE), which is supported by National Science Foundation grant number OCI-1053575.

Appendix: Evaluation of hyper-singular integral

We consider the numerical evaluation of the regularized integral involving the double normal derivartive of G_0 . Let

$$F(r,\theta) = \left(\frac{\partial^2 G_0}{\partial \bar{n}' \partial \bar{n}}\right) \left(p(\boldsymbol{r}_s,t_R') - p(\boldsymbol{r}_s',t') + \frac{\bar{R}}{c\alpha^2} \frac{\partial p}{\partial t}(\boldsymbol{r}_s,t_R')\right) |\mathbf{r}_{\xi} \times \mathbf{r}_{\eta}|$$

where (r, θ) is the polar coordinates for the local variable (ξ, η) centerred at the nodal point r'_s on element S_e . Denote the limit

$$\lim_{r \to 0} r^2 F(r, \theta) = G(\theta)$$

Then we have

$$\int_{S_{\epsilon}} F(r,\theta) dS = \lim_{\epsilon \to 0} \int_{0}^{2\pi} \int_{\epsilon}^{r(\theta)} F(r,\theta) r dr d\theta = \lim_{\epsilon \to 0} \int_{0}^{2\pi} \int_{\epsilon}^{r(\theta)} \left[\frac{r^{2} F(r,\theta) - G(0,\theta)}{r} + \frac{G(0,\theta)}{r} \right] dr d\theta$$

$$= \int_{0}^{2\pi} \int_{0}^{r(\theta)} \frac{r^{2} F(r,\theta) - G(0,\theta)}{r} dr d\theta + \lim_{\epsilon \to 0} \int_{0}^{2\pi} G(0,\theta) [\ln r(\theta) - \ln \epsilon] d\theta$$

$$= \int_{0}^{2\pi} \int_{0}^{r(\theta)} \frac{r^{2} F(r,\theta) - G(0,\theta)}{r} dr d\theta + \int_{0}^{2\pi} G(0,\theta) \ln r(\theta) d\theta$$

where we have used the fact that

$$\int_0^{2\pi} G(0,\theta)d\theta = 0$$

The final integral can be evaluated using high-order numerical quadratures.

References

- $^{1}\mathrm{C.~R.}$ Anderson, An implementation of the fast multipole method without multipoles, SIAM J. Sci. Comput., Vol. 13, 923-947, 1992.
- ²R. J. Astley and J. G. Bain, A three-dimensional boundary element scheme for acoustic radiation in low Mach number flows, Journal of Sound and Vibration, Vol. 109, 445-465, 1986.
- 3 L. Banjai, Multistep and multistage boundary integrals for the wave equation, Max-Planck Institute Preprint No. 58, 2010
- ⁴A. Boag, V. Lomakin and E Michielssen, Non-uniform grid time domain (NGTD) algorithm for fast evaluation of transient fields, IEEE trans. Antennas Propag., Vol. 54, 1943-1951, 2006.
- $^5\mathrm{S.}$ Borm, L. Grasedyck and W. Hackbusch, Introduction to hierarchical matrics with applications, Engineering Analysis with Boundary Elements, Vol. 27, 405-422, 2033
- ⁶A. Brandt, Multilevel computations of integral transforms and particle interactions with oscillatory kernels, Computer Physics Communications, Vol. 65, 24-38, 1991
- ⁷Y. Brick and A. Boag, "Multilevel nonuniform grid algorithm for acceleration of integral equation-based solvers for acoustic scattering", IEEE transaction on ultrasonic, ferroelectrics, and frequency control, Vol. 57, 261-273, 2010
- 8 O. M. Bucci, and G. Franceschetti, On the spatial bandwidth of scattered fields, IEEE Trans. Antennas Propag., Vol. 35, 1445-1455, 1987.
- ⁹A. J. Burton and G. F. Miller, The application of integral equation methods to the numerical solution of some exterior boundary-value problems, Proc.R.Soc.London, Ser A, Vol. 323, 201-210, 1971.
- ¹⁰D. J. Chappell, P. J. Harris, D. Henwood and R. Chakrabarti, "A stable boundary element method for modeling transient acoustic radiation", Journal of Acoustical Society of America, Vol. 120, No. 1, 74-80, 2006.
- ¹¹H. Chen, W. Y. Crutchfield, Z. Gimbutas, L. F. Greengard, J. F. Ethridge, J. Huang, V. Rokhlin, N. Yarvin, and J. Zhao, "A wideband fast multipole method for the Holmholtz equation in three dimensions", Journal of Computational Physics, Vol. 216, 300-325, 2006.
- ¹²M. Costabel, "Time-dependent problems with boundary integral equations", Encyclopedia of Computational Mechnics, E. Stein, R. de Borst and T. J. R. Hughes eds, John Wiley & Sons, 2004.
- ¹³M. H. Dunn and A. F. Tenetti, "Application of fast multipole methods to the NASA Fast Scattering code", AIAA paper 2008-2875, 2008
- ¹⁴A. A. Ergin, B. Shanker and E. Michielssen, "Analysis of transient wave scattering from rigid bodies using a Burton-Miller approach", Journal of Acoustical Society of America, Vol. 106, No. 5, 2396-2404, 1999.
- ¹⁵A. A. Ergin, B. Shanker and E. Michielssen, "Fast analysis of transient acoustic wave scattering from rigid bodies using the multilevel plane wave time domain algorithm", Journal of Acoustical Society of America, Vol. 107, No. 3, 1168-1178, 2000.
- ¹⁶F. Farassat and M. K. Myers, Extension of Kirchhoff formula to radiation from moving surfaces, Journal of Sound and Vibration, Vol. 123, 451-460, 1988.
- ¹⁷J. E. Ffowcs Williams and D. L. Hawkings, Sound generation by turbulence and surfaces in arbitrary motion, Phil. Trans. Royal Soc., Vol. 264A, 321-342, 1969.
- ¹⁸K. Fatahalian and M. Houston, A closer look at GPUs, Communications of the ACM, Vol. 51, No. 10, 50-57, 2008.
- ¹⁹M. B. Friedman and R. P. Shaw, Diffraction of pulses by cylindrical obstacles of arbitrary cross section, J. Appl. Mech., Vol. 29, 40-46, 1962.
- $^{20} \rm ftp://cmb24.larc.nasa.gov/outgoing/DPW4/$
- ²¹M. Garland and D. B. Kirk, Understanding throughput-oriented architectures, Communications of the ACM, Vol. 53, No. 11, 58-66, 2010.
- 22 L. Greengard and V. Rokhlin, "A fast algorithm for particle simulations", Journal of Computational Physics, Vol. 135, 280-292, 1997.
- ²³N. A. Gumerov and R. Duraiswami, Fast Multipole methods for the Helmholtz equations in three dimensions, Elsevier, 2004.
- ²⁴N. A. Gumerov and R. Duraiswami, "A broadband fast multipole accelerated boundary element method for the three dimensional Helmholtz equation", Journal of Acoustical Society of America, Vol. 125, 191-205, 2009.
- ²⁵N. A. Gumerov and R. Duraiswami, Fast multipole methods on graphics processors, Journal of Computational Physics, Vol. 227, 8290-8313, 2008.
- ²⁶Y. Guo, Slat noise modeling and prediction, Journal of Sound and Vibration, Vol. 331, 2567-2586,2012.
- 27 T Ha-Duong, B. Ludwig and I. Terrasse, A Galerkin BEM for transient acoustic scattering by an obstacle, Int. J. Numer. Meth. Eng., Vol. 57, 1845-1882, 2003.
- ²⁸W. Hackbusch, W. Kress and S. Sauter, Sparse convolution quadrature for time domain boundary integral formulations of the wave equation, IMA Journal of Numer. Anal., Vol. 29, 158-179, 2009
- ²⁹T. Hamada, T. Narumi, R. Yokota, K. Yasuoka, K. Nitadori and M. Taiji, 43 Tflops hierchical N-Body simulations on GPUs with applications in both astrophysics and turbulence, SC09 proceedings of the conference on high performance computing networking, storage and analysis, 2009.
- ³⁰F. Q. Hu, "A spectral boundary integral equation method for the 2D Helmholtz equation", Journal of Computational Physics, Vol. 120, 340-347, 1995.
- ³¹F. Q. Hu, "A fast numerical solution of scattering by a cylinder: spectral method for the boundary integral equations", Journal of Acoustic Society of America, Vol. 96, 3639-3703, 1994.
- 32 F. Q. Hu, X. D. Li, X. Y. Li and M. Jiang, Time Domain Wave Packet method and suppression of instability waves in aeroacoustic computations, AIAA paper 2011-2891, 2011

- ³³W. S. Hwang, Boundary spectral method for acoustic scattering and radiation problems, J. Acoust. Soc. Am., Vol. 102, 96-101, 1997.
- ³⁴H-W Jiang and J-G Ih, Stabilization of time domain acoustic boundary element method for the exterior problem avoiding the nonuniqueness, Journal of Acoust. Soc. Am, Vol. 133, 1237-1244, 2013.
- ³⁵A. D. Jones and F. Q. Hu, "An investigation of spectral collocation boundary element method for the computation of exact Green's function in acoustic analogy", AIAA paper 2006-2636, 2006.
- ³⁶A. D. Jones and F. Q. Hu, "A three-dimensional time-domain boundary element method for the computation of exact Green's functions in acoustic analogy", AIAA paper 2007-3479, 2007.
- ³⁷A. Klockner, T. Warburton, J. bridge, and J. S. Hesthaven, Nodal discontinuous Galerkin methods on graphics processors, Journal of Computational Physics, Vol. 228, 7863-7882, 2009.
- ³⁸D. Komatisch, G. Elerbacher, D. Goddeke and D. Michea, High-order finite element seismic wave propagation modeling with MPI on a large GPU cluster, Journal of Computational Physics, Vol 229, 7692-7714, 2010.
- ³⁹D. P. Lockard, An efficient, two-dimensional implementation of the Ffowcs Williams and Hawkings equation, Journal of Sound and Vibration, Vol. 229, 897-911, 2000.
- ⁴⁰S. Li, B. Livshitz and V. Lomakin, "Fast evaluation of Helmholtz potential on graphics processing units (GPUs)", Journal of Computational Physics, Vol. 229, 8463-8438, 2010.
- ⁴¹S. Li, B. Livshitz and V. Lomakin, Graphics Processing Unit accerelated O(N) micromegnetic solver, IEEE Transactions on Magnetics, Vol. 46, No. 6, 2373-2375, 2010.
- ⁴²L. Long, The compressible aerodynamics of rotating blades based on an acoust formulation, NASA TP 2197, 1983.
- 43 L. V. Lopes and C. L. Burley, Design of the next generation aircraft noise prediction program: ANOPP2, AIAA paper 2011-0840, 2011
- ⁴⁴Ch. Lubich, Convolution quadrature and discretized operational calculus. I, Numer. Math., Vol. 52, 129-145, 1988.
- ⁴⁵Ch. Lubich, On the multistep time discretization of linear initial boundary value problems and their boundary integral equations, Numer. Math., Vol. 67, 365-389, 1994.
- ⁴⁶D-J van Manen, J. O. A. Robertson and A. Curtis, Exact wave field simulation for finite-volume scattering problems, Journal of Acoustical Society of America, Vol. 122, EL115-EL121, 2007
- ⁴⁷J. Meng, A. Boag, V. Lomakin and E. Michielssen, "A multi-level Cartesian non-uniform grid time domain algorithm", Journal of Computational Physics, Vol. 229, 8430-8444, 2010
- ⁴⁸E. Michielssen, A. Boag, A multilevel matrix decompostion algorithm for analyzing scattering from large structures, IEEE Transactions on Antennas and Propagation, Vol. 44, 1086-1093, 1996.
- ⁴⁹K. M. Mitzner, Numerical solution for transient scattering from a hard surface of arbitrary shape retarded potential technique, J. Acoust. Soc. Am. Vol. 42(2), 391-397, 1967.
- ⁵⁰W. Mohring, Energy conservation, time reversal invariance and reciprocity in ducts with flow, Journal of Fluid Mech., Vol. 431, 223-237, 2001.
- ⁵¹W. R. Morgans, The Kirchhoff formula extended to a moving surface, Philol. Mag., Vol. 9, 141-161, 1930.
- ⁵²C. L. Morfey, Acoustic energy in non-uniform flows, Journal of Sound and Vibration, Vol. 14, 159-179, 1071.
- ⁵³L. Morino, Is there a difference between aeroacoutics and aerodynamics? An aeroelastician's view point, AIAA Journal, Vol. 41, 1209-1223, 2003.
- ⁵⁴P. M. Morse and K. U. Ingard, Theoretical Acoustics, Princeton, 1986.
- ⁵⁵M. K. Myers and J. S. Hausmann, On the application of the Kirchhoff formula for moving surfaces, Journal of Sound and Vibration, Vol. 139, 174-178, 1990.
- $^{56}\mathrm{M}$. K. Myers and J. S. Hausmann, Computation of acoustic scattering from a moving rigid surface, Vol. 91, 2594-2605, 1992.
- $^{57}\mathrm{NVIDIA},$ Compute Unified Device Architecture Programming Guide, 2008
- ⁵⁸A. R. Pilon and A. S. Lyrintzis, Development of an improved Kirchhoff method for jet aeroacoustics, AIAA Journal, Vol. 36, 783-790, 1998.
- ⁵⁹M. Schanz, T. Ruberg and L. Kielhorn, Time domain BEM: numerical aspects of collocation and Galerkin formulations, in *Recent advances in Boundary Element Methods*, Manolis and Polyzos (eds), Springer 2009.
- ⁶⁰R. P. Shaw, Transient scattering by a circular cylinder, Journal of Sound and Vibration, Vol. 42, 295-304, 1975.
- 61 H. A. Schenck: Improved Integral Formulation for Acoustic Radiation Problems, Journal of Acoustical Society of America , Vol. 44, 41-58, 1968.
- ⁶²A. Shlivinski and A. Boag, Multilevel surface decomposition algorithm for rapid evaluation of transient near-field to far-field transforms, IEEE Transaction of Antennas and Propagation, Vol. 57, 188-195, 2009.
- ⁶³S. F. Wu, Nonuniqueness of solutions to extended Kirchhoff integral formulations, Journal of Acoustical Society of America, Vol. 93, 683-695, 1993.
- ⁶⁴P. Zhang and T. W. Wu, A hypersingular integral formultion for acoustic radiation in moving flows, Journal of Sound and Vibration, Vol. 206, 309-326, 1997.
- ⁶⁵L. Ying, G. Biros, D. Zorin and H. Langston, A kernel-independent adaptive fast multipole algorithm in two and three dimensions, Journal of Computational Physics, Vol. 196, 591-626, 2004. Annalen
- ⁶⁶G. Yu, W. J. Mansur, J. A. M. Carrer and L. Gong, Stability of Galerkin and colocation time domain boundary element methods as applied to the scalar wave equation, Computers & Structures, Vol. 74, 495-506, 2000.
- ⁶⁷T, Takahashi and T. Hamada, GPU-accelerated boundary element method for Helmholtz equation in three dimensions, International Journal for Numerical Methods in Engineering, Vol. 80, 1295-1321, 2009.
- ⁶⁸R. Tsuchiyama, The OpenCL Programming Book, Fixstars Corp., 2010

 69 E. van't Wout, D. R. van der Heul, H. van der Ven and C. Vuik, Design of temporal basis functions for time domain integral equation methods with predefined accuracy and smoothness, IEEE Transactions on Antennas and Propagation, Vol. 61, 271-280.